Doctoral Dissertation (Shinshu University)

The fabrication and application of nanoparticle-based multifunctional composites

March 2021

LI XIAOJUAN

Abstract

Nanoparticle composites have attracted scientific attention due to the distinguished set of properties and applications. The properties of nanoparticles are dependent on the component size and structure. Therefore, the synthesis of nanoparticle composites with well component size, nanostructure, and morphology have attracted great interest. However, the controllable fabrication, and particular desired shape of nanoparticle-based composites are still a challenge. This thesis focuses on exploring the size-controllable, shape-controllable, and applications of nanoparticle-based composites. The nanostructure formation, properties and applications of composites are well discussed. The most significant results achieved in this dissertation are given as follows:

In this work, owing to the large surface area, graphene oxide (GO) was used as the carrier to protect nanoparticles from aggregating, and the π-π continuous surface can provide abundant ways for nanoparticles transferring during their application.

Silver nanoparticles/graphene oxide nanoscroll composites (Ag/GO nanoscroll composites) were fabricated by a one-step method at room temperature. The GO sheets were cut into pieces by the silver nanoparticles (AgNPs) due to their catalytic activity, and then the GO pieces rolled up, resulting from the intermolecular hydrogen bonds. Transmission electron microscope images show that the Ag/GO nanoscroll composites have open-ended tubular hollow structures. The Escherichia coli (E. coli) was used to evaluate the antibacterial activity of synthesized nanoscroll composites. After against the

E. coli for 3 days, the inhibition rate of Ag/GO nanoscroll composites can still up to 99.99%. This attributes to the open-ended tubular hollow structures, providing abundant channels and space to prevent AgNPs from aggregating and oxidizing. The result exhibits that the Ag/GO nanoscroll composites have the potential for long-lasting antibacterial activity. So, the Ag/GO nanoscroll composites can be applied in antibacterial materials for long-lasting use. On the other hand, the Ag/GO nanoscroll composites were synthesized as a recyclable photocatalyst. The open-ended nanoscroll structures provide sufficient space to prevent the AgNPs from oxidizing and aggregating, and the π-π continuous surface provides an abundance of pathways for AgNPs transfer during photodegradation. To demonstrate the recyclability of the synthesized photocatalytic composites, methylene blue aqueous solution was photodegraded under optimal conditions over ten consecutive photocatalytic cycles. The result shows that the Ag/GO nanoscroll composites are able to mineralize methylene blue to colorless within 10 min in each cycle, and no decomposition was detected after ten cycles. The Ag/GO nanoscroll composites can be used as a recyclable photocatalyst in wastewater treatment applications.

Additionally, Copper nanoparticles (CuNPs) have been widely studied because they are cheap and easy to be obtained. However, it is challenging to be long-term storage because of their oxidation in the air easily. To prevent CuNPs oxidation, the sandwich structure composites (CuNPs intercalated into graphene oxide (GO) sheets - CuNPs@GO composites) were fabricated via the liquid-phase reduction method. The limited GO interlayer distance controls the size of CuNPs (~ 10 nm in diameter) during the reduction

process, and the GO sheets serve as the protective cover to prevent CuNPs from oxidation. In addition, the large surface area of GO layer provides enough space for CuNPs against their aggregation. To confirm that the sandwich structure can protect CuNPs from oxidation, the air stability and high temperature stability of CuNPs@GO composites were evaluated. The result shows that the composites exhibit no oxidation sign following exposure to dry air for at least 21 weeks or 90 °C. Simultaneously, the conductivity result of the synthesized composites shows no change after exposure to dry air for at least 21 weeks. This sandwich structure provides a potential research direction for fabricating CuNPs with high antioxidant stability and stable conductivity.

Chapter 1

General introduction

Chapter 1: General introduction

1.1 Nanomaterials

Nanotechnology has gained huge attention in the past two decades, in which the nanomaterials are the primary and critical component. Nanomaterials are materials that have the size between 1 to 100 nm at least in one dimension and made up of carbon, metal, metal oxides, or organic matters [1]. Nanomaterials produce unique quality and capabilities by modifying the shape and size at the nanoscale level. Nanomaterials have different shapes, such as nanorods, nanoparticles, and nanosheets, based on their dimensionality [2]. The unique properties of nanomaterials, for example, high reactivity, strong sorption, etc., are explored for application in many fields like medicine [3-5], catalysis [6], renewable energy, and environmental remediation [7], and antibacterial material [8]. In this chapter, the classification, property, and application of nanomaterials are briefly introduced.

The nanomaterials are generally classified into the carbon-based nanomaterials, metal nanomaterials, nanocomposites, etc.

1.1.1 Carbon-based nanomaterials

The main constituent in this type of nanomaterials is carbon. They can be classified into graphene [9], carbon nanotubes (CNT) [10], carbon nanofibers [11, 12], fullerenes, and carbon dots [13]. Carbon-based nanomaterials are presented in Fig. 1-1.

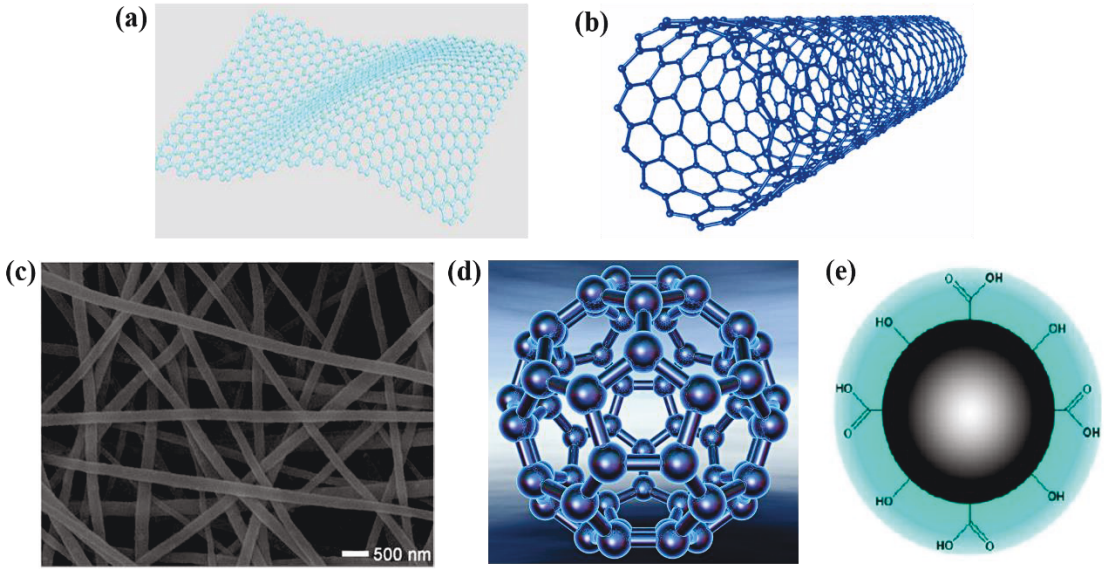

Fig. 1-1 Carbon-based nanoparticles. (a) graphene; (b) CNT; (c) carbon nanofibers; (d) fullerenes; (e) carbon dots.

Graphene, as one of the carbon-based nanomaterials, is the sheets of carbon atoms arranged in a hexagonal network. It was discovered in 2004 through a process of scotch tape peeling [14]. Owing to its properties such as high mobility of charge carriers, unique transport performance [15], high mechanical strength [16], and extremely high thermal conductivity and theoretically high surface area [17], graphene, as a 2D sheet of sp^2-hybridized carbon, suitable for many promising applications such as sensors [18], energy conversion devices [19], and catalysts [20]. The outstanding properties depend on the number of layers and dispersion performance of graphene sheets [21]. However, Van der Waals and π-π stacking interactions among individual graphene sheets result in their tendency to aggregate [22] when graphene dispersion solutions are dried. Therefore, preventing graphene agglomeration has become a significant research trend. A graphene layer interfacing with evenly distributed nanoparticles on the surface could lead to well-

defined, novel graphene with an exceptional surface area. The nanoparticles can act as a stabilizer against the aggregation of individual graphene sheets, which is generally caused by a strong Van der Waals interaction between graphene layers. Moreover, the graphene sheets decorated with nanoparticles might can result in some particular properties because they combine the outstanding properties of nanoparticles and the synergetic effect between them. At the present, the various kinds of nanoparticles [23-25] have been synthesized and supported on graphene, including Ag, Au, Cu, TiO_2, ZnO, etc.

Graphene oxide (GO) as a type of graphene is the product of chemical exfoliation of graphite and has been known for more than a century. GO has been known to disperse well in water since its first discovery over a century ago and thus has been routinely described as hydrophilic. The GO is the ideal alternative for the production of solution processable graphene, as it can be synthesized in large quantities from inexpensive graphite powder and can readily yield stable dispersions in various solvents. GO is an oxidized graphene sheet having its basal planes decorated mostly with epoxide and hydroxyl groups, in addition to carbonyl and carboxyl groups located at the edged.

1.1.2 Metal nanomaterials

There are different methods for the preparation of metal nanoparticles like chemical or photochemical methods. By using reducing agents, the metal ions are reduced to the metal nanoparticles. Almost all the metals can be synthesized into their nanoparticles [26]. The commonly used metals for nanoparticle synthesis are cobalt (Co), silver (Ag), copper

(Cu), gold (Au), iron (Fe), lead (Pb), zinc (Zn), etc. The nanoparticles have distinctive properties such sizes as low as 10 to 100nm, surface characteristics like a high surface area to volume ratio, pore size, surface charge and surface charge density, crystalline and amorphous structures, shapes like spherical and cylindrical and color, reactivity and sensitivity to environmental factors such as air, moisture, heat and sunlight etc. [27, 28]. Not only a single nanoparticle but also the mixing of two or more nanoparticles with size control can also be achieved. They are widely used in different research areas, environmental and bioimaging studies.

Among various metal nanomaterials, silver nanoparticles are obtained particular interests due to their unique properties, which could be used in broad-spectrum antimicrobial materials [29-31], chemical/biological sensors and biomedicine materials [32-34], and biomarker [35] and so on. They have unique optical, electrical, and thermal properties and are incorporated into the industrial application of electronics, catalysis, and photonics. Silver nanoparticles are one of the most attractive nanomaterials for commercialization applications. They have been used extensively as electronic products in the industry, antibacterial agents in the health industry, food storage, textile coatings, and environmental applications. As antibacterial agents, silver nanoparticles were used for a wide range of applications, from disinfecting medical devices and home appliances to water treatment [36-38]. However, the bare silver nanoparticles are prone to oxidize and aggregate while they are exposed to air or water at room temperature [39]. Therefore, the silver nanoparticles-based composite nanomaterials have become the current research

trend.

Since 1990s, copper nanoparticles have attracted much attention from scientists. Many techniques, such as chemical reduction [40], reduction of copper ions with supercritical fluids [41], and laser irradiation of copper oxide powders, are developed to synthesize copper nanoparticles [42, 43]. Copper nanoparticles have been pulled in extensive consideration because of their optical, catalytic, mechanical, and electrical properties [44, 45]. They have also been used as a substitute for gold, silver and platinum in different areas (e.g., thermal conducting materials and microelectronics applications) [46, 47]. However, copper nanoparticles have a large specific surface area and high chemical activity, which can be easily oxidized into dark red cuprous oxide and black copper oxide in the air, losing their original physical and chemical properties. In addition, the copper nanoparticles have low dispersion in the absence of modified stabilizers, which limits their application in many fields. Therefore, suitable base materials decorating copper nanoparticles to form nanocomposites point out a new direction for research.

1.1.3 Nanocomposites

The nanocomposite is a polyphase solid material where one of the phases has one, two, or three dimensions of less than 100 nm. Over recent years, nanocomposites have become a hot topic very fast by the reason of the quick development of nanofillers (nanoparticles, nanotubes, nano-whiskers, nanofibers, nanolayers and nanosheets) as well as the excellent material performances resulted from the great specific surface area, high

surface energy, small size effect, quantum benefit and macroscopic quantum tunneling of nanofillers. In them, the graphene-based nanocomposites are developing in recent days to a large extent. The single-layer carbon atoms are arranged in a hexagonal matrix, with zero band gap. The electrons are almost as the massless particles that consist of the good electrical medium in 2D [48]. The oxidation product of graphene is graphene oxide, whose electronic conductivity is excellent [49]. The different types of graphene oxide family nanocomposites are metal/graphene oxide nanoparticles, metal oxide /graphene oxide nanocomposites, metal chalcogenide/graphene oxide nanocomposites. The metal and metal oxides possess a variety of applications. Among of them, Ag [50], Cu [51], Au [52], ZnO [53], TiO_2 [54], and Fe_2O_3 [55] show the photocatalytic, photovoltaic, drug delivery [56], gas sensors [2], batteries [57] and cytotoxicity activities [58].

1.2 Antibacterial materials

Bacterial contamination has become a crucial problem due to many infections in food storage, medical implants, hospital settings, biosensors, and public health events [59]. Therefore, antibacterial materials have been widely researched. Antibacterial material refers to a new type of functional material that kills or inhibits bacteria. Many substances have good bactericidal or antimicrobial functions, such as some organic compounds with specific groups, some inorganic metal materials and their compounds, and some minerals. However, antibacterial materials are functional materials that can inhibit or kill surface

bacteria by adding individual antibacterial agents, such as antibacterial plastics, antibacterial fibers, and fabrics, antibacterial Ceramics, antibacterial metal materials, etc.

1.2.1 Organic antibacterial agents

The main varieties of organic antibacterial agents are vanillin or ethyl vanillin compounds, which are often used in polyethylene food packaging films to have an antibacterial effect. In addition, the acylanilides, imidazoles, thiazoles, isothiazolone derivatives, quaternary ammonium salts, bisquats, phenols, etc. are also used as antibacterial agents. Generally, organic antibacterial agents have low heat resistance, are easily hydrolyzed, and have a short validity period. Simultaneously, the safety of organic antibacterial agents is still under research.

1.2.2 Inorganic antibacterial agents

There are many types of inorganic antibacterial agents, such as Ag, Cu, and ZnO, which can bring antibacterial activity to materials. Sevinc etc. [60] have demonstrated that the blending 10 wt.% ZnO nanoparticles into dental composites displays antibacterial activity and reduces the growth of bacterial biofilms against Streptococcus subrings by roughly 80% for a single-species model dental biofilm. In addition, a variety of metallic biocides used for mold inhibition are only operative for the short-term. Therefore, the development of simple, low-cost, and long-term effective antibacterial methods is significant.

1.2.3 Nano antibacterial agents

Nano antibacterial materials are the treatment of inorganic antibacterial agents with high-tech nanotechnology so that they have more extensive and excellent antibacterial and sterilization functions; it improves the long-term antibacterial effect through the slow release. Nanoparticles are widely used as antibacterial activities mainly through two reactions. The first one is called the contact reaction, which relies on Cullen's gravity to attach nano ions to cell walls firmly, then the nano ions can break through the cell walls and enter the cells to solidify the bacterial protein [61, 62]; eventually the cells die due to loss of the ability to divide and multiply. When the bacteria lose their activity, nano ions are freed out from the bacteria, repeated sterilization, so their antibacterial effect can last a long time. The second one is called the photocatalytic reaction, meaning that under the action of light, nano ions activate the water and air of oxygen adsorbed to the surface of the powder, producing OH^- and O_2^-, which can decrease the ability of bacteria to multiply and destroy bacteria in a short period of time.

Among all the nanoparticles, silver nanoparticles with a high bactericidal activity [63, 64] have been widely applied in medicine to prohibit colonization of bacteria on prostheses [65], wound-dressing [66], and to reduce infections in burn treatment [67]. However, the bare silver nanoparticles are prone to oxidize and aggregate while exposed to air or water [39]. To overcome the shortcomings, many other materials, such as carbon nanotubes (CNTs), graphene oxide (GO), and so forth, have been employed as potential support materials to increase the stability and antibacterial activity of silver nanoparticles

[68-73]. Among these materials, the one-dimensional CNTs have been widely used as adsorbents to remove various environmental pollutants due to their unique structures and high super physical and chemical properties. CNTs have high electron transfer property, making them have better photocatalytic performance and yield an efficient antibacterial activity level. However, the CNTs tend to agglomerate due to their hydrophobic nature, limiting some applications. In contrast, GO has received significant interest due to a large number of oxygen bonds, such as hydroxyl, carboxyl and epoxide groups, which stabilize the aqueous dispersion of GO [74-76] can be a suitable support material to increase the stability of silver nanoparticles.

1.3 Photocatalytic materials

1.3.1 History of photocatalytic materials

The history of photocatalysis can be traced back to the 1960s. The discovery of water photolysis on a TiO_2 electrode by Fujishima [77] and Honda in 1972 has been recognized as the landmark event that stimulated the investigation of photonic energy conversion by photocatalytic methods [78, 79]. Since then, intense research has been carried out on TiO_2 photocatalysis, which focused on understanding the fundamental principles, enhancing the photocatalytic efficiency, and expanding the scope of applications [80]. Unfortunately, TiO_2 is not ideal for all purposes and performs relatively poorly in processes associated with solar photocatalysis. In principle, TiO_2 can utilize no more than 5% of the total solar

energy impinging on the earth' surface due to its wide bandgap (3.2 eV). Therefore, during the past decade, much effort has been devoted to modifying TiO_2 and investigated possible alternatives to TiO_2.

1.3.2 Semiconductor photocatalytic materials

Semiconductor photocatalytic materials have received much attention as a potential solution to the world energy shortage and counteract environmental degradation. In semiconductors, the conduction-band electrons (e_{cb}^-) have a chemical potential of + 0.5 to -1.5 V versus the normal hydrogen electrode (NHE); hence they can act as reductants. The valence-band holes (h_{vb}^+) exhibit a strong oxidative potential of + 1.0 to + 3.5 V versus NHE [81]. The energy of the incident photons is stored in the semiconductor by photoexcitation, then converted into chemical form by a series of electronic processes and surface/interface reactions.

TiO_2 photocatalyst, as one of the traditional semiconductor materials, is widely used in a variety of applications and products in the environmental and energy fields, including self-cleaning surfaces, air and water purification systems, sterilization, hydrogen evolution, and photoelectrochemical conversion. The photocatalytic properties of TiO_2 are derived from the formation of photogenerated charge carriers (hole and electron), which occurs upon the absorption of ultraviolet light corresponding to the band gap [82, 83]. The photogenerated holes in the valence band diffuse to the TiO_2 surface and react with adsorbed water molecules, forming hydroxyl radicals (•OH). The photogenerated

holes and the hydroxyl radicals oxidize nearby organic molecules on the TiO_2 surface. Electrons in the conduction band typically participate in reduction processes, which typically react with molecular oxygen in the air to produce superoxide radical anions ($\bullet O_2^-$). However, only a small proportion of the holes is trapped at lattice oxygen sites and may react with TiO_2, which weakens the bonds between the lattice titanium and oxygen ions. As a result, the effect achieved by TiO_2 photocatalysis is not very significant. ZnO photocatalyst presents higher photocatalytic activity than TiO_2 in the photodegradation of some organic compounds, so it is a suitable alternative to TiO_2 [84]. However, the photocatalytic activity of ZnO is still not high enough because the low separating efficiency of the photoelectron hole pairs and the structure of the ZnO crystal would be destroyed after consecutive use due to the photo corrosion effect.

1.3.3 Novel photocatalytic materials

In order to overcome these drawbacks, a lot of efforts have been made to improve or replace the traditional semiconductor photocatalysts. Recently, the introduction of noble metal nanoparticles (e.g., Ag, Au) onto semiconductor surfaces contributes to expanding the light-harvesting scope of UV and visible light, due to their potent surface plasmon resonance (SPR) effects [85]. In addition, owing to their low Fermi levels, noble metal nanoparticles might serve as electron trappers, reducing the photogenerated electron-hole recombination rate [86]. Among the noble metals, Ag is considered to be the most economical raw material with the most potent SPR effect. Ag as a co-catalyst

could enhance the separation of electron-hole. Thus, the photocatalytic activity of the semiconductor increased. It can be inferred that Ag can be a potential candidate for photocatalysis.

1.4 Purpose of this research

Nanotechnology is one of the most active research areas with both novel science and useful applications. Nanotechnology is a multidisciplinary science which deals with physics, chemistry, materials science, and other engineering sciences. The applications of nanotechnology are spreading in almost all branches of science and technology. So far, the research of nanotechnology has made specific achievements; however, nanoparticle composites with controllable shape and size are still challenging in the present study. In this thesis, thence, three different types of nanoparticle-based composites with controlled shapes and sizes were investigated. (1): The Ag/GO nanoscroll composites were synthesized using a one-step method at room temperature, where the GO sheets were cut into pieces by AgNPs (4 - 10 nm), and then rolled up to nanoscrolls due to the force of intermolecular hydrogen bonds. The synthesized the Ag/GO nanoscroll composites can be applied as an antibacterial material and a recyclable photocatalyst for long-lasting use. (2): The sandwich shaped CuNPs@GO composites were fabricated via the liquid-phase reduction method, in which the limited GO interlayer distance controls the CuNPs growth (~ 10 nm diameter) during the reduction process, and the GO sheets serve as the protective

cover to prevent CuNPs from oxidation. The sandwich composites exhibit no sign of oxidation after exposure to dry air for at least 21 weeks or 90 °C heat and show stable conductivity after at least 21 weeks' exposure to dry air.

The research schematic for this work is shown in Fig. 1-2.

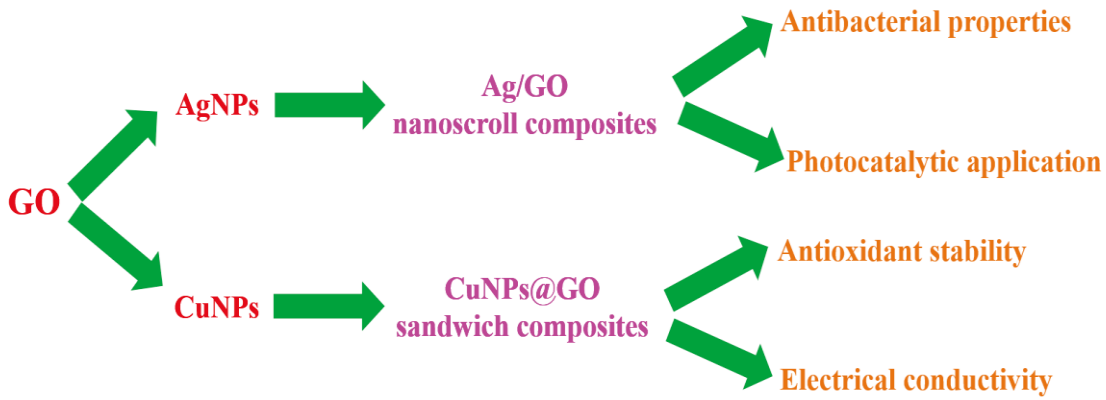

Fig. 1-2 The research schematic

Chapter 2

The synthesis and antibacterial activity of silver nanoparticles/graphene oxide nanoscroll composites

Chapter 2: The synthesis and antibacterial activity of silver nanoparticles/graphene oxide nanoscroll composites

2.1 Introduction

Graphene nanoscrolls (GNSs), a new type of graphene family materials, is an important carbon material with a one-dimensional tubular structure [87-91]. GNSs inherit some excellent properties of both graphene and carbon nanotubes (CNTs) [92], such as outstanding electrical conductivities, high mechanical strength, and high carrier mobility [90, 93, 94]. They have been used as hydron storage [95, 96] and batteries [97, 98]. In addition, owing to their open-ended topological tubular structures, GNSs are expected to possess some properties distinct from graphene and CNTs [99, 100]. Compared with graphene, the electrons and molecules can quickly diffuse into or onto the tubular walls of GNSs at high rates. Their open-ended structures can accommodate as many as molecules during the intercalation process without breaking tubular walls [101]. Compared with multiwalled carbon nanotubes (MTCNTs), the elections flow within a single nanoscroll rather than through several coaxially nested nanoscrolls [102, 103]. To date, many efforts have been done to theoretical predict and calculate GNSs[100, 102, 104], but the synthesis of GNSs by various methods is still restricted from the technical difficulties [94, 103]. In chemical methods, the complex experimental process

dramatically increases the cost and wastes energy [105-107]. The harsh experimental conditions in physical methods make it harder to isolate the GNSs from raw materials such as graphite and carbon [108-110]. Besides, the technique of rolling up graphene can fabricate GNSs. The experiments are based on multiple operation steps, which needs several days, and the efficiency is low[92, 102, 111]. Graphene oxide (GO) has received significant attention owing in no small number of oxygen functional bonds. These abundant oxygen groups assist the dispersion of GO in water as a stable suspension. Owing to this property, GO can provide active sites to functionalize and hybridize with other materials[112]. However, there have been few reports on graphene oxide nanoscrolls, which is fabricated by rolling up graphene oxide sheets.

Silver nanoparticles (AgNPs) have attracted considerable research interests because of their antibacterial activities [113-115]. The large surface area of AgNPs allows them to contact with the bacteria in a better way; then the AgNPs can break through the cell walls and enter the cells to solidify the bacterial protein [61, 62]. Eventually the cells die due to loss of the ability to divide and multiply. On the other hand, AgNPs can activate the oxygen in water and air adsorbed to the surface of the powder, producing OH^- and O_2^-, which can decrease the ability of bacteria to multiply and destroy bacteria in a short period of time [116, 117]. However, the bare AgNPs are prone to oxidize and aggregate while they are exposed to air or water [39]. Therefore, the AgNPs-based composite antibacterial agents must be fabricated to enhance the application of different kinds of bacteria.

Here, to simplify the practical steps and increase the efficiency, silver nanoparticles/

graphene oxide nanoscroll composites (Ag/GO nanoscroll composites) were fabricated by a one-step method at room temperature. The GO sheets were cut into pieces by AgNPs in the nitrogen atmosphere, and then, the pieces of GO sheets were rolled up by the force of intermolecular hydrogen bonds. To study the rolling up conditions, three different molar ratios (R) of GO solution to silver nitrate ($AgNO_3$) were carried out. Under the optimal condition, the Escherichia coli (E. coli) was used to evaluate the antibacterial activity of synthesized composites. It was owing to the open-ended tubular hollow structures, which can provide abundant channels and space to prevent AgNPs from aggregating and oxidizing, that the Ag/GO nanoscroll composites have the potential for long-lasting antibacterial activity. As a result, the Ag/GO nanoscroll composites can be applied in antibacterial materials for long-lasting use.

2.2 Experimental

2.2.1 Materials and reagents

Graphite flake (median 7-10 micron) was obtained from Alfa Aesar a Johnson Matthey Co., Ltd. Sulfuric acid (H_2SO_4), potassium permanganate ($KMnO_4$), hydrogen peroxide (H_2O_2), hydrochloric acid (HCl), silver nitrate ($AgNO_3$), trisodium 2-hdroxypropane-1,2,3-tricarboxylate (Na_3Ct) and 2-dimethylaminoethanol (DMEA) were all purchased from Wako Pure Chemical Co., Ltd (Osaka, Japan). Escherichia (E. coli) and related reagents were all obtained from Nantong University, China. All chemicals

were analytical reagents and used without further treatments. Deionized water was used throughout the course of the investigation.

2.2.2 The fabrication of Ag/GO nanoscroll composites

2.2.2.1 The synthesis of GO

GO was synthesized by a modified Hummers method [118]. First, graphite flake powder (1g) was added into H_2SO_4 solution (23mL, 99%) under stirring in an ice bath. While the powder was completely dissolved, $KMnO_4$ (3g) was added very slowly, keeping the suspension temperature lower than 5°C. After that, the system was transferred to oil bath (40 °C) and stirred for 30 min. Then, 50 mL of deionized water was added, and the system was stirred at 95°C for 15min. Another 150 mL of deionized water was added, followed by addition of H_2O_2 (5mL, 30%), the color of the solution turned from dark brown to bright yellow. Finally, the mixture was washed with HCl solution (1:10, 150mL) to remove metal ions. The solution was purified by filtering until PH is 7. Thereafter, the solution was washed by ultrasonic for 30 min to exfoliate it to GO. To remove the unexfoliated graphite, the dispersion was centrifuged for 30 min (3500 rpm).

2.2.2.2 The synthesis of Ag/GO nanoscroll composites

The Ag/GO nanoscroll composites were synthesized by a one-step approach using $AgNO_3$ as AgNPs precursor, and GO solution was used both as dispersant and carrier for

AgNPs. The $AgNO_3$ was dissolved in the GO solution. Then, an aqueous solution of Na_3Ct was added dropwise, keeping the mixture stirring at room temperature. Followed by the DMEA added to the reaction mixture, the mixture was then stirred for one hour at room temperature. The color of the mixture changed from bright yellow to pale brown. Finally, the mixture was washed twice and separated by centrifugation (5000 rpm) to remove impurities and re-dispersed in deionized water to obtain the silver nanoparticles/graphene oxide nanoscroll composites. Three different molar ratios (R) of GO solution to $AgNO_3$ were carried out. The specific contents of reagents for the experimental operation are shown in Table 2-1.

Table 2-1 The specific contents of reagents

	R=0.5	**R=1**	**R=2**
$AgNO_3$	2.94 mmol	5.88 mmol	11.76 mmol
GO	42 mL	42 mL	42 mL
Na_3Ct	0.147 mmol/mL	0.294 mmol/mL	0.588 mmol/mL
DMEA	58.8 mmol/mL	117.6 mmol/mL	235.2 mmol/mL

2.2.3 Antibacterial activity test

The antibacterial activity of Ag/GO nanoscroll composites was evaluated by a colony count method, taking place under the optimal condition. E. coli was employed for different antibacterial assays[119-121]. In the colony count method [122], The E. coli (2 mL, 10^4 CFU/mL) was inoculated in 50 mL PBS with 0.75 g of as-prepared samples

(control, graphene oxide (GO), silver (Ag), carbon nanotubes (CNTs), Ag/GO nanoscroll composites). The mixtures were incubated in a rotary shaker at 150 rpm and 37 °C for 20 - 24 h. Then, 100 μL of above suspensions (final concentration: 3 μg/mL) were uniformly spread over the surface of the agar solution and put in an incubator at 37 °C. The bacterial growth was monitored at an interval of 12 h over three days. The antibacterial activity was evaluated by counting the colonies.

2.2.4 Instruments and characterizations

2.2.4.1 Morphology

The Ag/GO nanoscroll composites were dried for morphological measurement and analysis. Field-emission scanning electron microscopy (FE-SEM) images of Ag/GO nanoscroll composites were obtained from a Hitachi S-5000 operating at 20kV. Transmission electron microscopy (TEM) images were acquired by a JEOL JEM 2010 TEM operating at 200kV. The distribution of elements was carried out on a Hitachi S-3000N scanning electron microscopy (SEM) equipped with an EX-200 EDS.

2.2.4.2 Chemical structure characterization

X-ray diffraction (XRD) measurements were performed on a MiniFlex 300 XRD using Cu Kα radiation. UV-vis (UV-2700 Spectrophotometer, Shimadzu Co., Ltd., Japan) was used to obtain the absorption spectra of GO and Ag/GO nanoscroll composites.

Fourier transform infrared spectroscopy (FT-IR) was used to analyze the chemical structures of GO and Ag/GO nanoscroll composites, using an IR Prestige-21 Spectrometer (Shimadzu Co., Ltd., Japan), with the transmit method. The element contents were carried out on a Hitachi S-3000N scanning electron microscopy (SEM) equipped with an EX-200 EDS.

2.2.4.3 Antibacterial standards

Based on GB 15979-2002 Sanitary Hygiene Products Hygiene Standards, Appendix C5[123-125] non-dissolving antibacterial, the antibacterial activity of the obtained samples was investigated by the colony count method.

2.3 Results and discussion

2.3.1 Determination of the optimal condition

Three different molar ratios (R=0.5, R=1, and R=2) of GO solution to $AgNO_3$ were carried out to obtain the optimal rolling up condition. The morphology and nanostructure of Ag/GO nanoscroll composites were investigated by FE-SEM and TEM (Fig. 2-1). The results show that when R is 1, the GO sheets were cut into pieces, and then, the GO pieces rolled up to nanoscrolls with 100 nm in diameter (Fig. 2-1(c)) and Fig. 2-1(d)), attached by lots of AgNPs. Compared with R = 0.5 (Fig. 2-1 (a) and 2-1(b)), the diameter of the nanoscroll composites in R=1 is smaller (100 nm < 300 nm). This result can be explained

as that the diameter of nanoscrolls is depended on the size of GO pieces, and the size of GO pieces is determined by the number of silver nanoparticles. Compared with R = 0.5, the number of AgNPs is much more in R = 1 due to more $AgNO_3$ content. Therefore, a larger number of carbon-carbon bonds are broken due to more silver nanoparticles, and the size of GO pieces is smaller. Compared with R is 2 (Fig. 2-1(e), 2-1(f)), the GO sheets in R=1 are cut into pieces, and then roll up successfully. The failure of rolling up conditions in R=2 is because the AgNPs with high density are aggregated on the surface of pieces of GO sheets (Fig. 2-1(f)), exceeding the limit of the intermolecular hydrogen bonds. The synthesized Ag/GO nanoscroll composites in our method (Fig. 2-1(g)) show four intense peaks at $2\theta = 38.1°$, 44.3°, 64.4°, and 77.5°, which are respectively assigned for (111), (200), (220) and (311) lattice planes of Ag [75], which are in agreement with the standard card (JCPDS: 04-0783) [126]. Compared with R=0.5 and R=2, all the peaks in R=1 are the sharpest, indicating that the highest quality are characterizes the AgNPs. As shown in Fig. 2-2 (a) and Fig. 2-2 (b), the size of AgNPs in R=1 is from 4-10 nm, which indicates that the AgNPs have excellent nanomaterial properties. The EDS area mapping (Fig. 2-2 (c-e)) was used to investigate the homogeneity of the contained elements. The result shows that the distribution of AgNPs filled inside and outside of Ag/GO nanoscroll composites is even with high density. Overall, these results exhibit that R=1 is the optimal condition to fabricate Ag/GO nanoscroll composites.

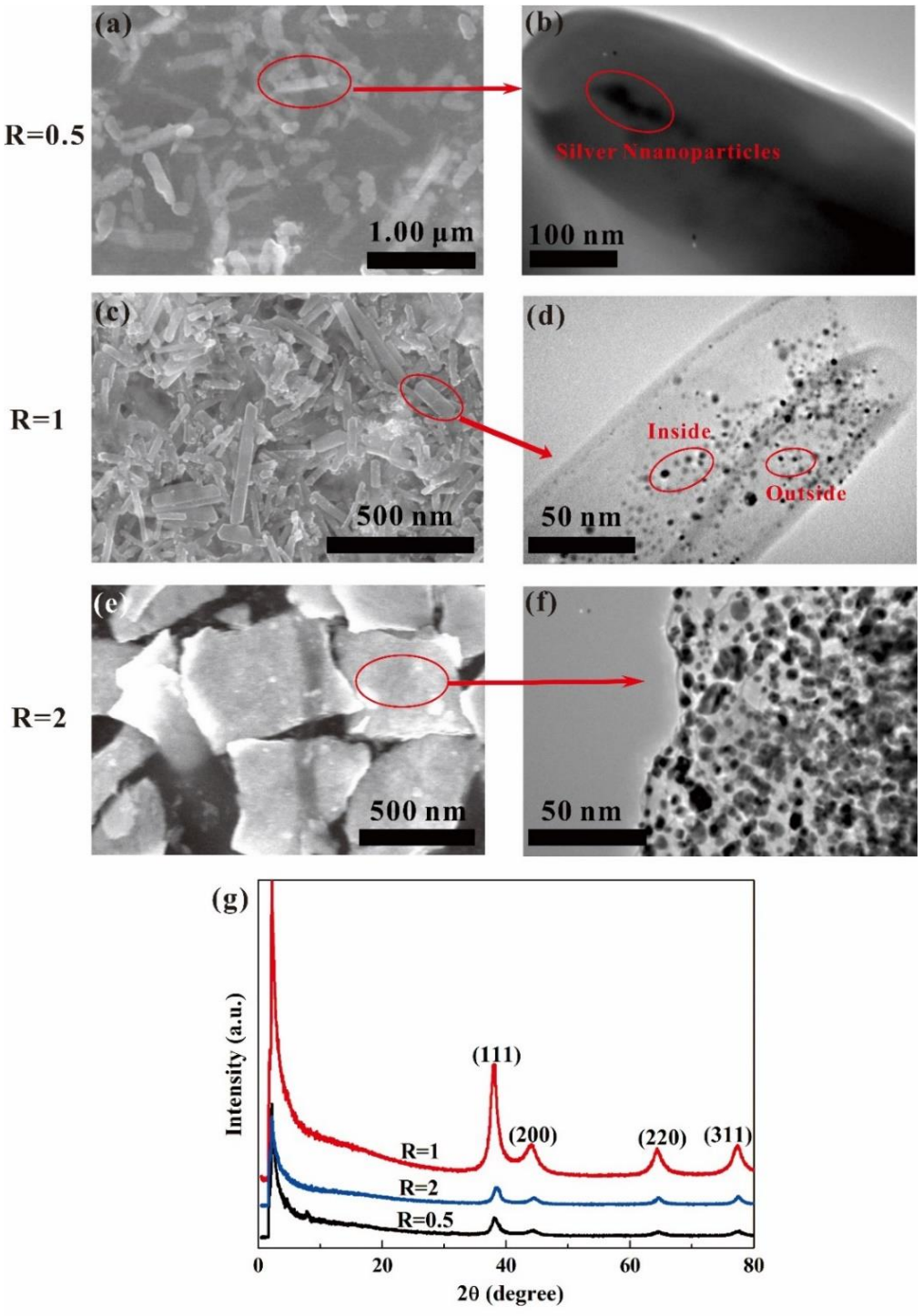

Fig. 2-1 Analysis of three different molar ratios of Ag/GO nanoscroll composites. (a), (b) R=0.5; (c), (d) R=1; (e), (f) R=2. (a), (c) and (e) FE-SEM images; (b), (d) and (f) TEM images; (g) XRD pattern of three different molar ratios of Ag/GO nanoscroll composites.

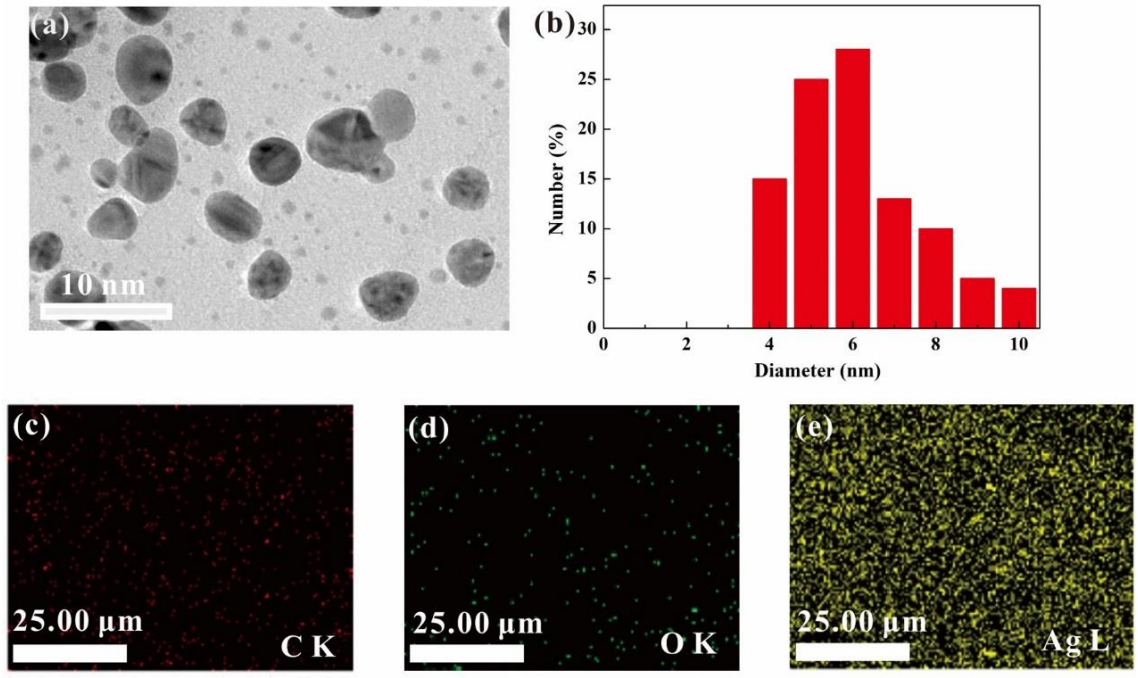

Fig. 2-2 Analysis of R=1. (a) TEM image of AgNPs; (b) Size distribution histogram of AgNPs; (c), (d) and (e) Area mapping analysis for each element present in R=1.

2.3.2 Analysis of the Ag/GO nanoscroll composites

GO is amphiphilic with a lot of hydroxyl groups (-OH) and carboxyl groups (-COOH) located at the edges and the defective sites [127]. As shown in Fig. 2-3, The SEM micrograph (Fig. 2-3 (a)) exhibits that the radial dimension of the GO sheet is on the order of several hundred to several micrometers. In Fig. 2-3 (b), the sharp peak at $2\theta=2.22°$ corresponds to an interlayer distance of 3.98 nm (d_{001}) according to Bragg Formula ($2d \sin\theta = n\lambda$). Compared with literature reports [128, 129], the prepared GO in our work has a higher degree of oxidation [130]. As a result, the GO made in our work has abundant oxygen groups. As illustrated in Fig. 2-4, when $AgNO_3$ was dispersed in GO

solution (5 wt.%) under stirring, the silver ions dispersed homogeneously in the GO solution. After the reductant (Na_3Ct) was added, the silver ions in the mixture solution were exchanged with the counterions (Na^+) via the ionic exchange mechanism, and silver ions were reduced to the form AgNPs, attached on the surface of GO sheets. When the DMEA was dropped to the above mixture, some C-C bonds were broken and the GO sheets were cut into pieces (compare the size of GO in Fig. 2-3 (a) and nanoscrolls in Fig. 2-1 (c)) because the AgNPs act as a catalyst to form transition-metal complexes under the nitrogen atmosphere [131-133]. Meanwhile, the electrostatic attraction between positive-charge hydrogens (H) and more electro-negative of oxygens (O), the powerful intermolecular hydrogen bonds (O – H ⋯ O) are formed at the edges of the pieces of GO sheets. Due to the force of intermolecular hydrogen bonds, the pieces of GO sheets were rolled up. As reported [134], the intermolecular hydrogen bonds could make the density of the electron more uniform in the infrared light, making the spectra shift to the lower frequency. Compared with the GO spectra (Fig. 2-5), the O-H vibration peaks of the Ag/GO nanoscroll composites shift from 3410 cm^{-1} and 1634 cm^{-1} to 3254 cm^{-1} and 1458 cm^{-1}, respectively. The result shows that the pieces of GO sheets were rolled up by the force of intermolecular hydrogen bonds.

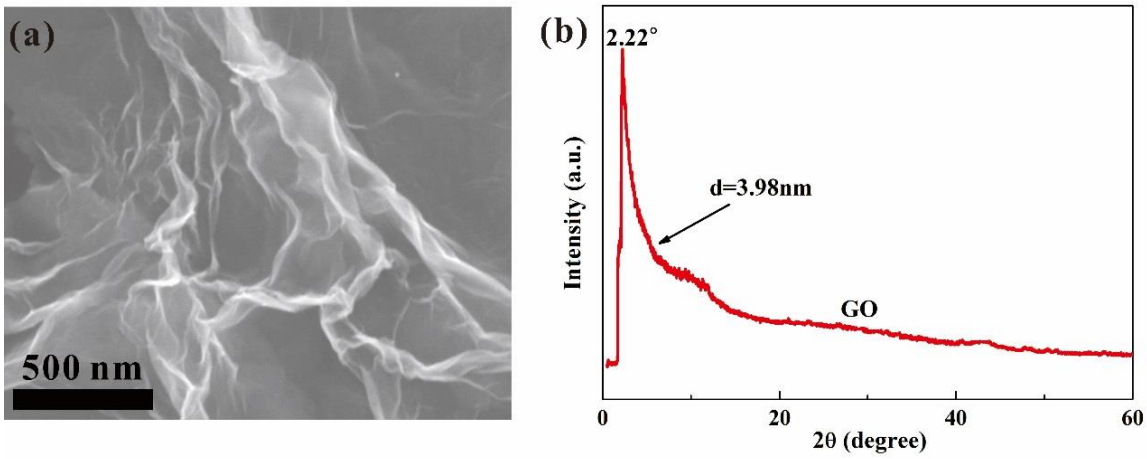

Fig. 2-3 (a) SEM image of GO; (b) XRD pattern of GO.

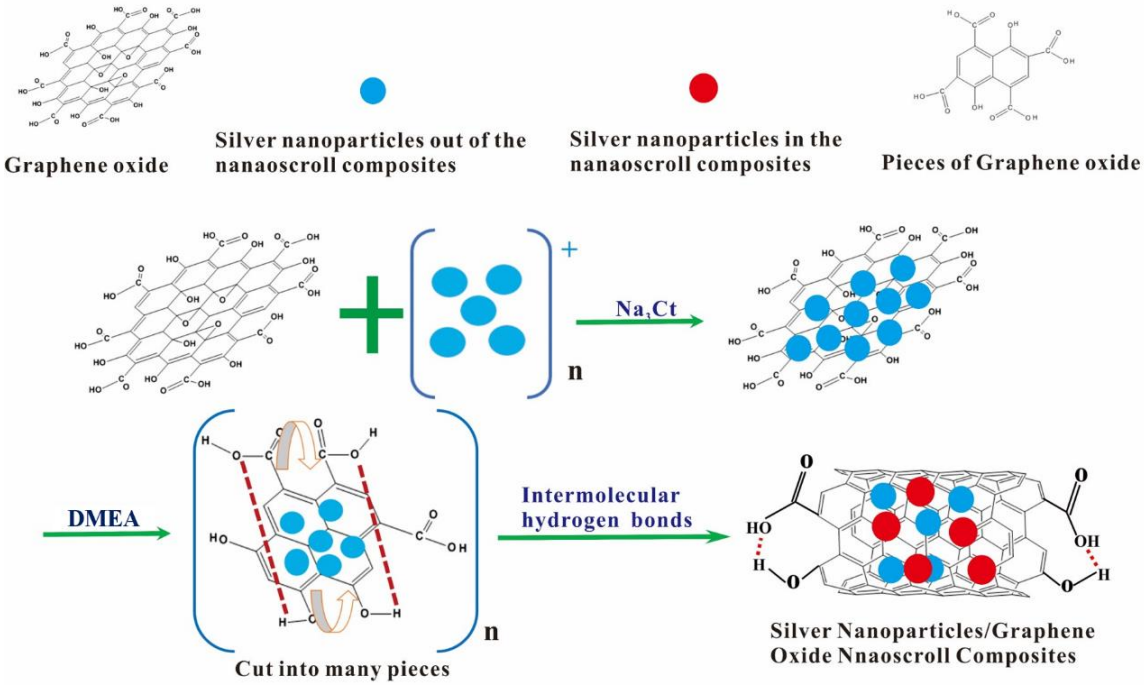

Fig. 2-4 Schematic illustration of the silver nanoparticles/graphene oxide nanoscroll composites synthesis process.

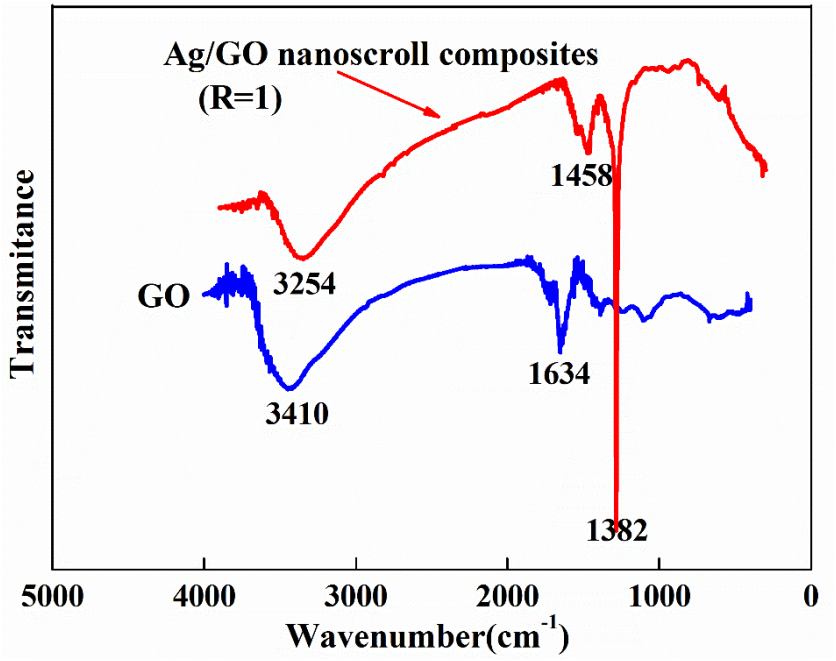

Fig. 2-5 FT-IR spectra of GO and Ag/GO nanoscroll composites (R=1).

In order to prove that the properties and composition of GO have not been changed after the one-step approach, the comparison analysis under the optimal condition has been done by XRD, UV-vis, and EDS. In Fig. 2-6 (a), compared with the GO curve, the sharp peak at $2\theta = 2.22°$ in Ag/GO nanoscroll composites curve does not show any change, which exhibits that the crystallinity of GO does not change during the rolling up process. The UV-vis transmittance spectra of GO and Ag/GO nanoscroll composites are illustrated in Fig. 2-6 (b). Two clear peaks can be observed in the spectra of Ag/GO nanoscroll composites, compared with the GO spectra. Plasmon resonance (SPR) band is observed at 410 nm confirms the Ag ions have been reduced into AgNPs, which is consistent with literature values[131, 135]. In particular, compared with the curve of GO, a new transmission peak at 330 nm appears in the curve of Ag/GO nanoscroll composites. This

maybe because, in Ag/GO nanoscroll composites, the UV light can easily pass through the open-ended tubular hollow structures, forming a transmission peak, while the sheets of GO prevent the UV light from transmitting. The EDS (Fig. 2-6 (c)) result shows that the atomic ratio of carbon to oxygen in the GO is consistent with that in the Ag/GO nanoscroll composites, which further confirms that the rolling up process in this chapter does not change the composition of GO. This is because the reducibility of Na_3Ct is not strong enough and the reaction process was carried out at room temperature, which does not meet the conditions for reducing GO. As a result, the GO was not reduced.

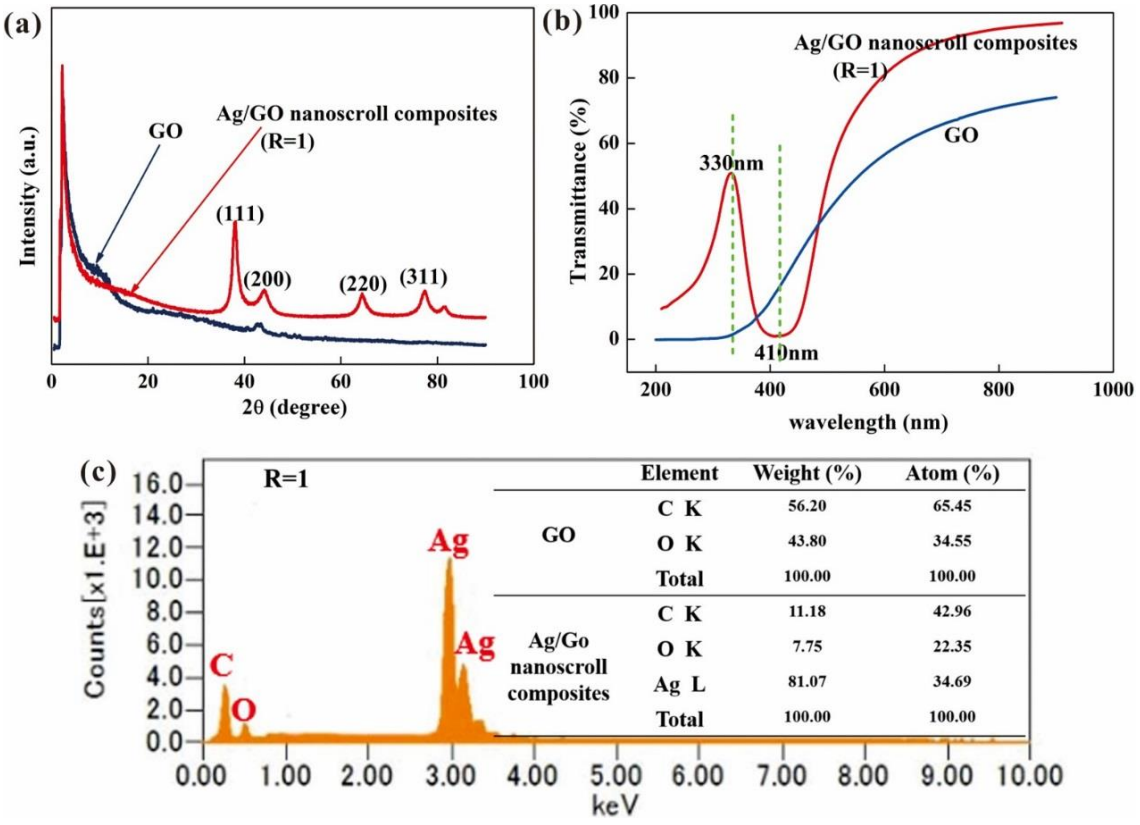

Fig. 2-6 Comparison analysis of GO and Ag/GO nanoscroll composites. (a) XRD pattern; (b) UV- vis transmittance spectra; (c) EDS results.

2.3.3 The effect of temperature on AgNPs and Ag/GO nanoscroll composites

The rate of reaction increased with increasing reaction temperature, resulting in the formation of larger AgNPs [135]. In the investigation, the synthetic reaction of Ag/GO nanoscroll composites was performed at 50°C (R=1). It can be observed that the reaction mixture of the product turned brown more quickly than that at room temperature. Fig. 2-7 (a) shows a TEM image of Ag/GO nanoscroll composites obtained at 50°C. As temperature rises, the size of AgNPs attached on the surface of GO gets bigger (ranges from 30 to 40 nm in diameter). It is noted that the GO sheets cannot be scrolled up, suggesting that the formation process is also depended on the size of AgNPs. Additionally, from EDS spectrum (Fig. 2-7 (b)), the atomic ratio of AgNPs prepared at room temperature is higher than that at 50°C. However, the atomic ratio of carbon to oxygen is essentially the same at two different conditions. This result indicates that the structure and properties of the GO are not affected by heating condition. Although the composition of the GO cannot affect by the temperature, the sizes of the AgNPs become larger with increasing temperature, and the AgNPs are aggregated on the GO sheets, resulting the failure of formation process of Ag/GO nanoscroll composites.

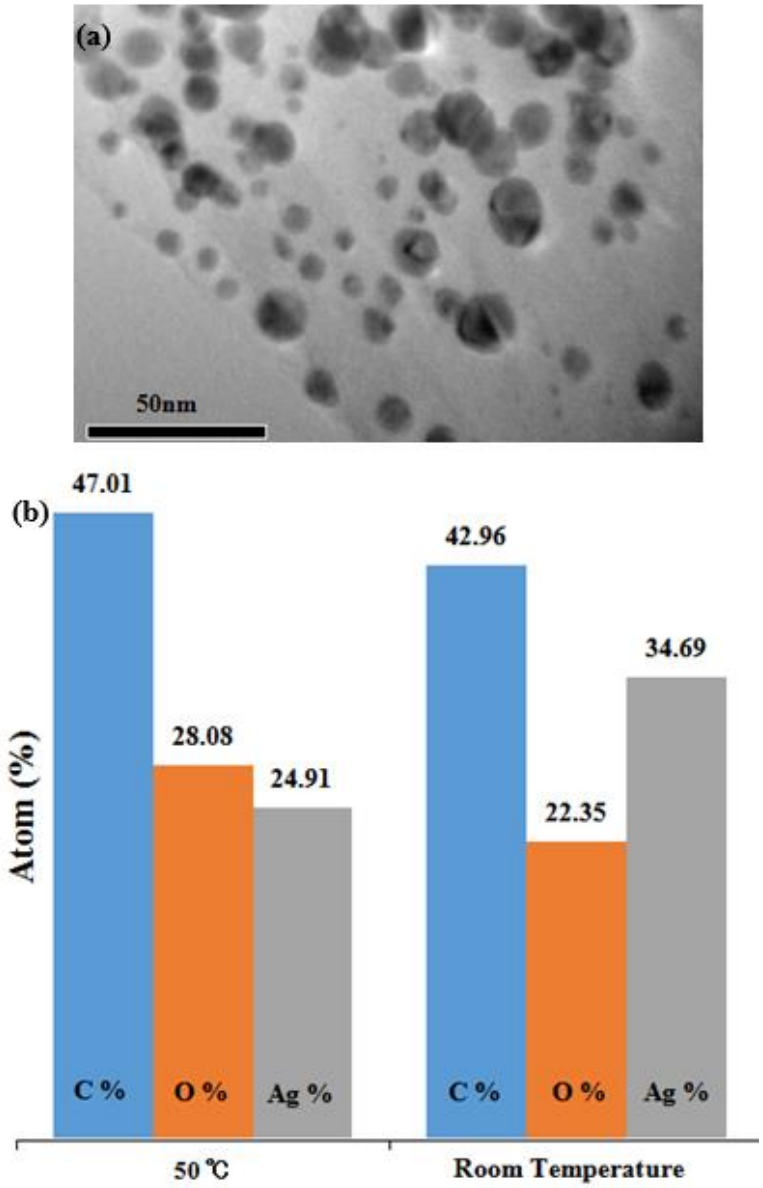

Fig.2-7 Preparation of Ag/GO nanoscroll composites (R=1) at 50 °C. (a) TEM image of Ag/GO nanoscroll composites; (b) EDS analysis of Ag/GO nanoscroll composites.

2.3.4 Antibacterial activity of the Ag/GO nanoscroll composites

The colony count method was used to quantitatively evaluate the long-lasting antibacterial activities of Ag/GO nanoscroll composites compared with the blank, GO, Ag and CNTs against the E. coli for 3 days. The inhibition rates are shown in Fig. 2-8.

Compared with the control test (Fig. 2-8 (a)), different samples exhibit antibacterial activities in the order: Ag/GO nanoscroll composites > Ag > CNTs > GO. In particular, the inhibition rate of the Ag/GO nanoscroll composites (Fig. 2-8 (e)) can still remain to 99.99% over 3 days. This is because the open-ended tubular hollow structures provide enough space to prevent the AgNPs from aggregating and oxidizing, and the π-π electrons are continuous in the nanoscrolls which can provide abundant channels for AgNPs to transport quickly and efficiently. As a result, the Ag/GO nanoscroll composites exhibit long-lasting antibacterial activity. The bacteria digital photos (after 3 days) of different samples are shown in Fig. 2-9.

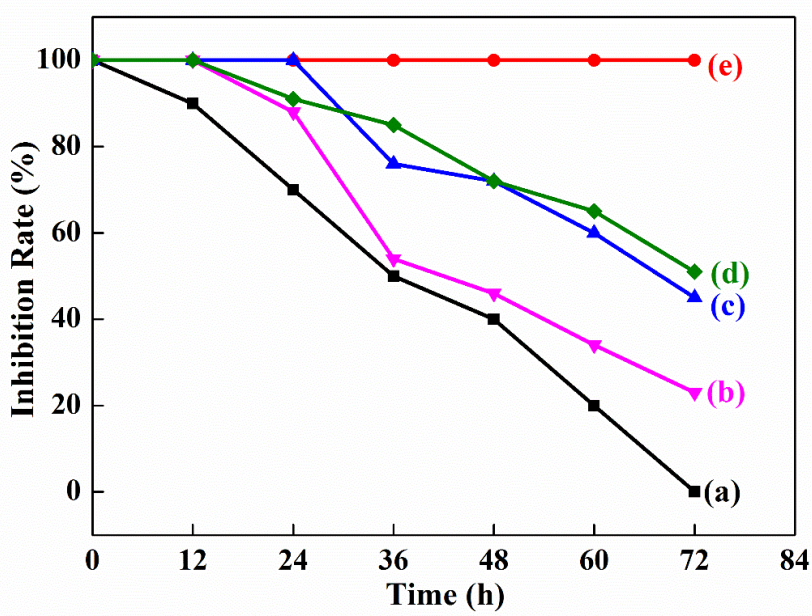

Fig. 2-8 The inhibition rate against E. coli. (a): control test; (b): GO; (c): CNTs; (d): Ag; (e): Ag/GO nanoscroll composites. Incubation condition: 37 °C, 3 days.

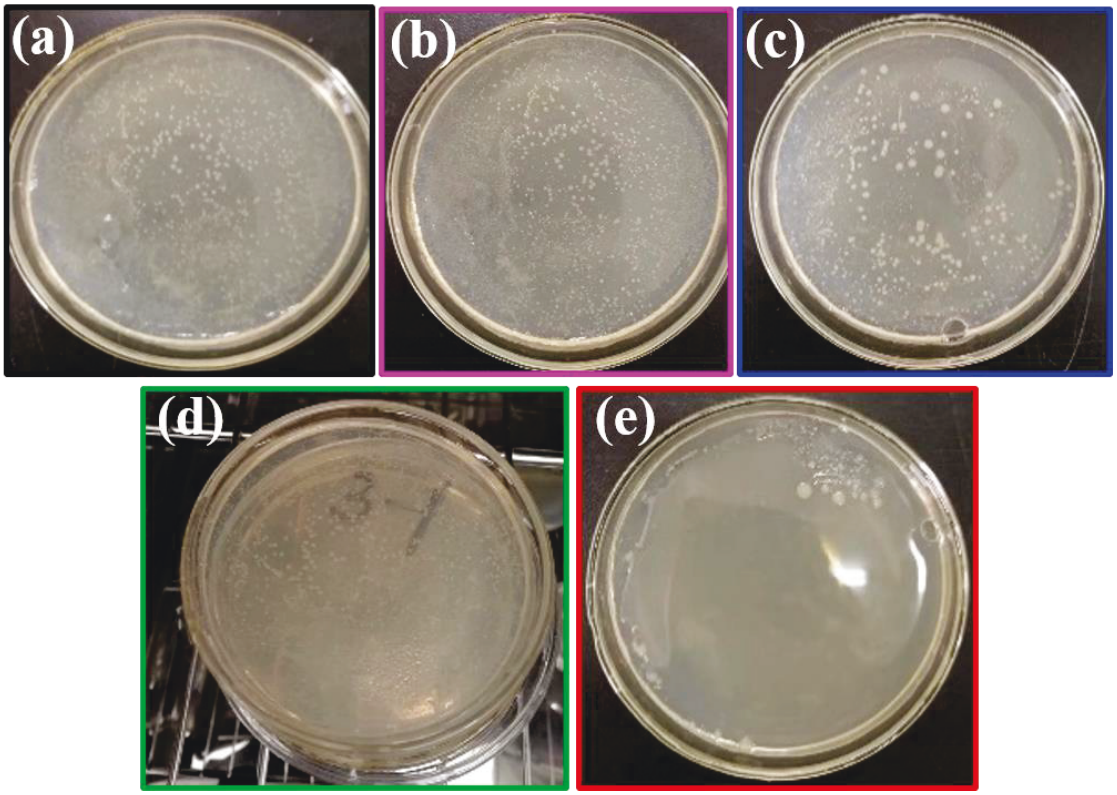

Fig. 2-9 The bacteria digital photos (after 3 days) of different samples. (a): control test; (b): GO; (c): CNTs; (d): Ag; (e): Ag/GO nanoscroll composites.

2.4 Conclusions

In summary, the Ag/GO nanoscroll composites were fabricated by a one-step method with a short time and high efficiency. The GO sheets were cut into pieces by AgNPs under the nitrogen atmosphere. Three different molar ratios were carried out to study the optimal condition of the rolling up process. The result shows that when the $AgNO_3$ of 5.88 mmol was added into the GO solution of 42 mL at room temperature, the GO sheets were cut into pieces, and then, the Ag/GO nanoscroll composites of 100 nm in diameter are

fabricated by the force of intermolecular hydrogen bonds, attached by lots of AgNPs with 4 - 10 nm in size. Throughout the rolling up process, the properties and composition of the GO have not changed. The E. coli was used to evaluate the long-lasting antibacterial activity of the Ag/GO nanoscroll composites. The result shows that after against the E. coli for 3 days, the inhibition rate of Ag/GO nanoscroll composites can still up to 99.99%. This is due to their open-ended tubular structures, and the composites provide abundant continuous channels and space to prevent the AgNPs from aggregating and oxidizing, which enhance the antibacterial activity of the composites to use for a long time. As a result, the Ag/GO nanoscroll composites can be applied as antibacterial materials for long-lasting use.

Chapter 3

The photocatalytic application of silver nanoparticles/graphene oxide nanoscroll composites

Chapter 3: The photocatalytic application of silver nanoparticles/graphene oxide nanoscroll composites

3.1 Introduction

With rapid economic growth and industrialization, the environmental pollution caused by organic and inorganic wastes and hazardous metal has become an overwhelming problem worldwide [136-138]. Dyes are commonly used to color products in the textile industries; however, most dye molecules used do not bind to fibers [139, 140]. Therefore, many dyes are therefore released into the water system, resulting in harm to the environment and human and animal health [141-144]. Photocatalysis is considered one of the most effective methods of removing organic pollutants from wastewater [145-150]. Recently, nanomaterials have been used as adsorbents in photocatalysis owing to their high surface area [151]. As a consequence of their catalytic properties, silver nanoparticles (AgNPs) are considered as one of the most promising nanomaterial catalysts [152-155]. However, agglomeration and oxidation limit their reuse in photocatalysis [156]. To overcome these problems, suitable substrates such as polymers, metal oxides, and graphene materials are used to disperse the AgNPs by forming composite photocatalysts [157-159].

Graphene oxide (GO) is one of the suitable substrates used to adsorb dyes because it can improve the transfer rate of conduction band electrons and has a high surface area [160-162]. In addition, GO has a large number of oxygen functional bonds that assist the

dispersion of GO in water to form a stable suspension. Owing to these properties, GO can be functionalized and hybridized with AgNPs to produce excellent composites. Nevertheless, because GO has a two-dimensional flat structure, it does not prevent AgNPs from oxidizing, which limits the reuse of the composites for subsequent photocatalytic processes [163]. GO nanoscrolls, which form nanoscroll composites with AgNPs, offer better photocatalyst recyclability than GO. This is attributed to the one-dimensional nanoscroll structures that can wrap AgNPs to prevent them from oxidizing and provide sufficient space to prevent AgNPs from agglomerating. However, there have been few reports on the synthesis and properties of GO nanoscrolls combined with AgNPs.

In this chapter, considering the huge photocatalytic potential, the AgNPs are used as the photocatalyst for photodegradation of MB. Simultaneously, to reduce the negative impact of agglomeration of AgNPs, GO are used as the carrier and protective agent to prevent AgNPs from agglomeration and oxidation. In addition, in order to protect the AgNPs from oxidation in long-term photodegradation use, the two-dimensional GO sheets are rolled up to one-dimensional nanoscrolls. Therefore, Ag/GO nanoscroll composites were synthesized for use as a recyclable photocatalyst. The controlled variable method, degradation sample (GO, AgNPs, Ag/GO nanoscroll composites), bath ratio of sample to methylene blue (MB) solution (1:100, 1:200, 1:300), initial MB concentration (100 mg/L, 200 mg/L, 300 mg/L), and light source (UV light, natural sunlight), was used to obtain the optimal conditions for photodegradation. In addition, to demonstrate the recyclability of the Ag/GO nanoscroll composite photocatalyst, ten consecutive cycles under the optimal conditions were comprehensively studied.

3.2 Experimental

3.2.1 Materials, reagents and synthesis of Ag/GO nanoscroll composites

As reported in our previous work, the GO was synthesized by the modified Hummers method [118]. The Ag/GO nanoscroll composites were synthesized by a one-step approach. The entire experiment was performed at room temperature. Firstly, the $AgNO_3$ was dissolved in the GO solution, followed by an aqueous solution of Na_3Ct added dropwise. Then, the DMEA was added to the reaction mixture, the mixture was then stirred for one hour. The color of the mixture changed from bright yellow to pale brown. Finally, the mixture was washed twice and separated by centrifugation to remove impurities and re-dispersed in deionized water.

3.2.2 Photocatalytic activity evaluation

3.2.2.1 Establishing the optimal photocatalytic conditions

The optimal photocatalytic conditions for the Ag/GO nanoscroll composites were established by photodegradation of MB solution at room temperature. Different degradation samples (GO, AgNPs, Ag/GO nanoscroll composites), different bath ratios of sample to MB solution (1:100, 1:200, 1:300), different initial MB concentrations (100 mg/L, 200 mg/L, 300 mg/L), and different light sources (UV light, natural sunlight), were assessed using the controlled variable method. First, the catalyst samples were added to the MB solutions and stored in the dark for 24 h to attain the adsorption-desorption equilibrium between the MB solution and the samples [164]. Subsequently, the first

sample (at 0 min) was taken out, and light irradiation was started. At certain time intervals, 3 mL samples were taken and centrifuged at 5000 rpm for 10 min to remove the particles. The supernatants obtained were analyzed using UV-vis spectroscopy. The absorbance of a characteristic band at 664 nm (λ_{max}) [165] was determined by measuring in the wavelength range 400 - 800 nm.

3.2.2.2 Photocatalytic recyclability evaluation

To demonstrate the recyclability of the Ag/GO nanoscroll composite photocatalyst, ten consecutive cycles were carried out under the optimal conditions. After each cycle, the sample was filtered to separate the catalyst from the MB solution, repeatedly washed with deionized water, and dried at 50°C before the next photocatalysis cycle.

The concentration C (mg/L) and the photodegradation rate D (%) were evaluated using a calibration curve based on the absorbance of the dye at various known concentrations [166] of MB, given by :

$$D = \frac{(C_0 - C_t)}{C_0} \times 100\% \quad (3\text{-}1)$$

where c_0 is the initial concentration of MB and c_t is the concentration of MB at time t.

3.2.3 Instruments and characterization

The Ag/GO nanoscroll composites were dried for morphological measurement, analysis, and photodegradation. The morphology of the Ag/GO nanoscroll composites was determined from the Transmission electron microscopy (TEM) images acquired using a JEOL JEM 2010 TEM operating at 200kV. Energy dispersive spectroscopy (EDS)

was carried out on a Hitachi S-3000N scanning electron microscope equipped with an EX-200 EDS. UV-vis spectroscopy (UV-2700 Spectrophotometer, Shimadzu Co., Ltd., Japan) was used to determine the absorption spectra of the MB solution at certain time intervals. The samples were centrifuged using an H-27F centrifuge (Kokusan, Japan). X-ray diffraction (XRD) measurements were performed on a MiniFlex 300 XRD using Cu Kα radiation. Fourier transform infrared spectroscopy (FT-IR) was used to analyze the chemical structures of the decolorized solution, using an IR Prestige-21 Spectrometer (Shimadzu Co., Ltd., Japan) with an ATR accessory. The UV light source (300 W mercury lamp; λ = 365 nm) was purchased from Shanghai Lanpu Light, China. The conditions for natural sunlight exposure were: 9:00 to 15:00 on December 26, 2019, in Ueda, Japan.

3.3 Results and Discussion

3.3.1 Optimization of photocatalysis conditions for the Ag/GO nanoscroll composites

The optimal photocatalytic conditions were established using the controlled variable method. Several experiments were carried out to study the influence of a variety of factors on the photocatalytic performance of the Ag/GO nanoscroll composites.

3.3.1.1 Effect of degradation sample

Fig. 3-1 shows the photocatalytic activities of different samples (a)-(d). For the blank sample (Fig. 3-1(a)), in the absence of photocatalyst, no changes in the MB absorption spectrum were observed, indicating that MB was not degraded at all. Compared with the

blank sample, GO (Fig. 3-1 (b)) shows a gradual decrease in MB absorption over 8 h. This is attributed to the large surface area of GO that can uniformly adsorb MB molecules. However, the adsorbed particles reduce the light transmittance of GO as time progresses, resulting in a decrease in photocatalytic efficiency. As shown by the AgNPs spectra (Fig. 3-1 (c)), the AgNPs initially show excellent photocatalytic activity for mineralizing MB, but subsequently was almost unchanged after 4 h. AgNPs can effectively degrade MB, but due to agglomeration and photo-corrosion, AgNPs gradually lose their photocatalytic activity over time. In contrast, the Ag/GO nanoscroll composites (Fig. 3-1 (d)) exhibit effective photodegradation, and the MB is mineralized to colorless within 8 min. This performance is attributed to the open-ended nanoscroll structures with π-π continuous surfaces, which provide an abundance of pathways for AgNPs to transfer during photodegradation. The UV light can be absorbed quickly and efficiently by the AgNPs and the electrons in the valence band of the Ag/GO nanoscroll composites can be excited to the conduction band [167], resulting in that a large number of electron-hole (e^- - h^+) pairs being generated. The photoelectrons and holes transfer quickly to the surfaces owing to the π-π continuous surfaces. The holes can react with water (H_2O) or hydroxide (OH^-) at the surfaces of the composites to generate hydroxyl radicals (·OH) with strong oxidation properties. On the other hand, photoelectrons can also interact with oxygen (O_2) on the surface to generate superoxide radicals ($\cdot O_2^-$), followed by further reactions to generate ·OH. Owing to the high activity of ·OH, the MB is degraded to water (H_2O) and carbon dioxide (CO_2). The process of photodegradation using the Ag/GO nanoscroll composites is illustrated in Scheme 3-1, and the specific reaction equations are as follows

[168, 169] :

$$\mathrm{Ag} + \mathrm{h}\nu \rightarrow \mathrm{Ag} + e^- + h^+ \quad (3\text{-}2)$$

$$H_2O + h^+ \rightarrow H^+ + \cdot OH \quad (3\text{-}3)$$

$$OH^- + h^+ \rightarrow \cdot OH \quad (3\text{-}4)$$

$$O_2 + e^- \rightarrow O_2^- \quad (3\text{-}5)$$

$$O_2^- + H^+ \rightarrow \cdot HO_2 \quad (3\text{-}6)$$

$$2 \cdot HO_2 \rightarrow H_2O_2 + O_2 \quad (3\text{-}7)$$

$$H_2O_2 + O_2^- \rightarrow O_2 + OH^- + \cdot OH \quad (3\text{-}8)$$

$$\cdot\mathrm{OH} + \mathrm{MB} \rightarrow H_2O + CO_2 + Inorganic\ molecules \quad (3\text{-}9)$$

As shown in Fig. 3-1(e), the photodegradation rates of GO, AgNPs, and Ag/GO nanoscroll composites reached 24.12%, 38.25%, and 99.99%, respectively, after 8 h under UV light irradiation. The Ag/GO nanoscroll composites show a highly efficient photodegradation of MB.

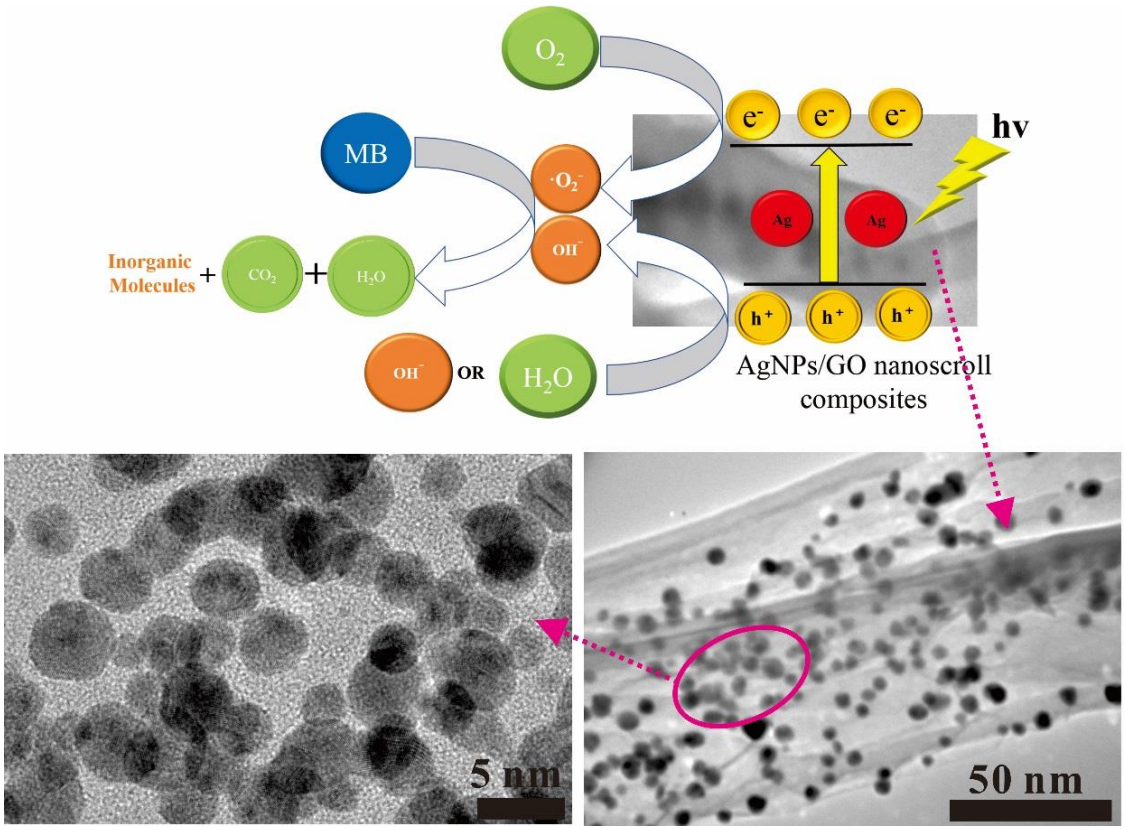

Scheme 3-1 The photodegradation process of the Ag/GO nanoscroll composites.

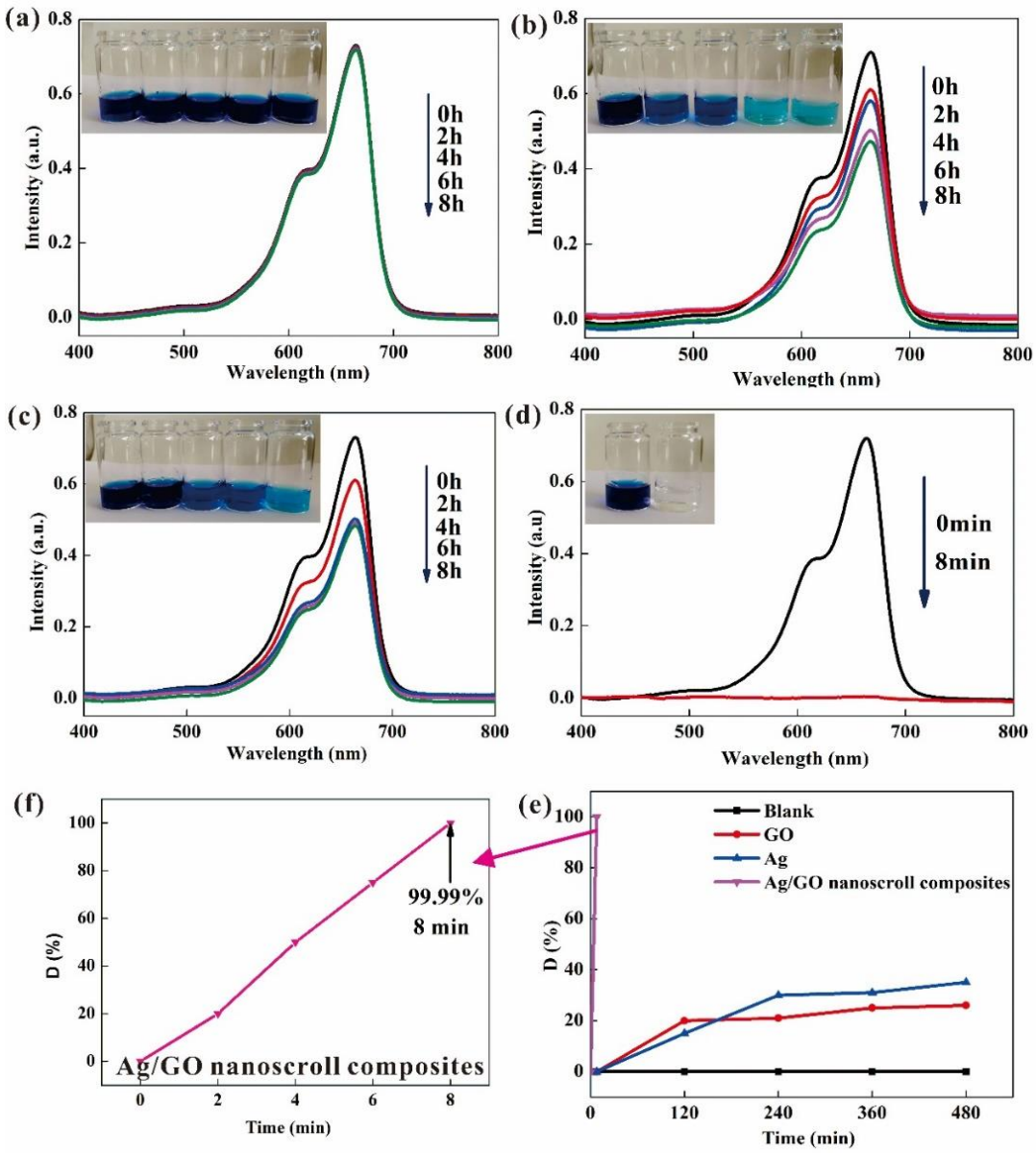

Fig. 3-1 Effect of degradation samples. (a) - (d) absorption spectra change for different degradation samples: (a) blank; (b) GO; (c) AgNPs; (d) Ag/GO nanoscroll composites. (e) photodegradation rate for the degradation samples. (f) magnification of the Ag/GO nanoscroll composites photodegradation curve. The suspension color changes are shown in the insets of (a) - (d). (conditions: bath ratio of sample to MB solution 1:100, initial MB concentration of 100 mg/L, and UV light irradiation).

3.3.1.2 Effect of initial MB concentration

As shown in Fig. 3-2(a) - (c), when the initial MB concentration was increased from 100 mg/L to 200 mg/L and 300 mg/L keeping other parameters constant, the mineralization time increased from 8 min to 15 min and 20 min, respectively. The photodegradation rate (Fig. 3-2 (d)) reached 99.99% for each initial concentration. The result shows that the Ag/GO nanoscroll composites achieved high photocatalytic activity even when the initial MB concentration was 300 mg/L. This is because the increase in the initial concentration presents the increase of MB organic molecules, which increases mineralization time.

The increase number of MB molecules means an increase in the number of molecules that need to be degraded. In this case, the required oxidant increases, which increases the photodegradation time. However, an increase in photodegradation time does not mean a decrease in photodegradation efficiency. This is because that the generated hydroxyl radicals ($\cdot OH$) and superoxide radicals ($\cdot O_2^-$) are much more than the MB molecules under this condition.

It was therefore concluded that 100 mg/L is the best initial MB concentration for photodegradation.

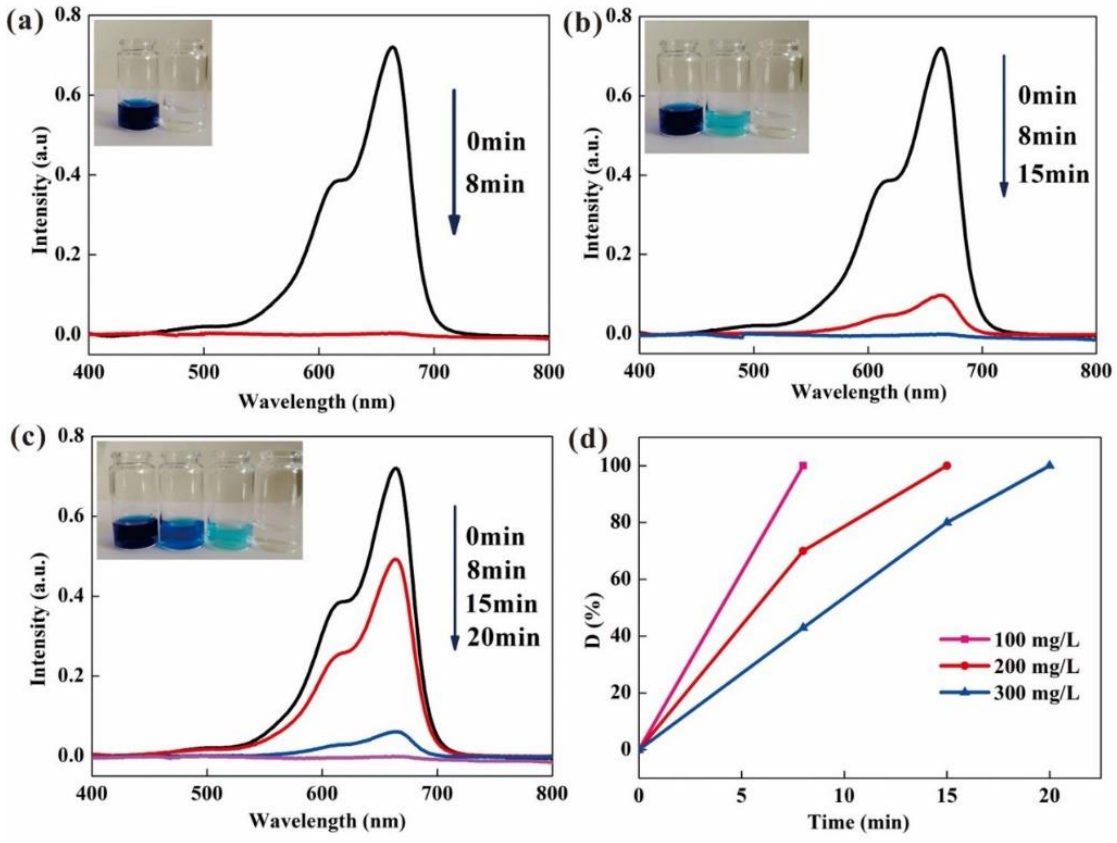

Fig. 3-2 Effect of initial MB concentration. (a) - (c) absorption spectra change for different initial MB concentrations: (a) 100 mg/L; (b) 200 mg/L; (c) 300 mg/L. (d) photodegradation rates for the different initial MB concentrations. The suspension color changes are shown in the insets of (a) - (c). (conditions: bath ratio of Ag/GO nanoscroll composites to MB solution 1:100 and UV light irradiation).

3.3.1.3 Effect of bath ratio of Ag/GO nanoscroll composites to MB solution

As shown in Fig. 3-3(a) - (c), MB was mineralized to colorless in all cases. An increase in bath ratio led to more MB being mineralized. The results show that the time for complete photodegradation of MB increased from 8 min to 13 min and 19 min with bath ratios of 1:100, 1:200, and 1:300, respectively, and the photodegradation rates all reached 99.99%. Therefore, increasing the bath ratio only increased the total

photodegradation time without affecting the degradation efficiency of the Ag/GO nanoscroll composites. In short, the best bath ratio condition is 1:100.

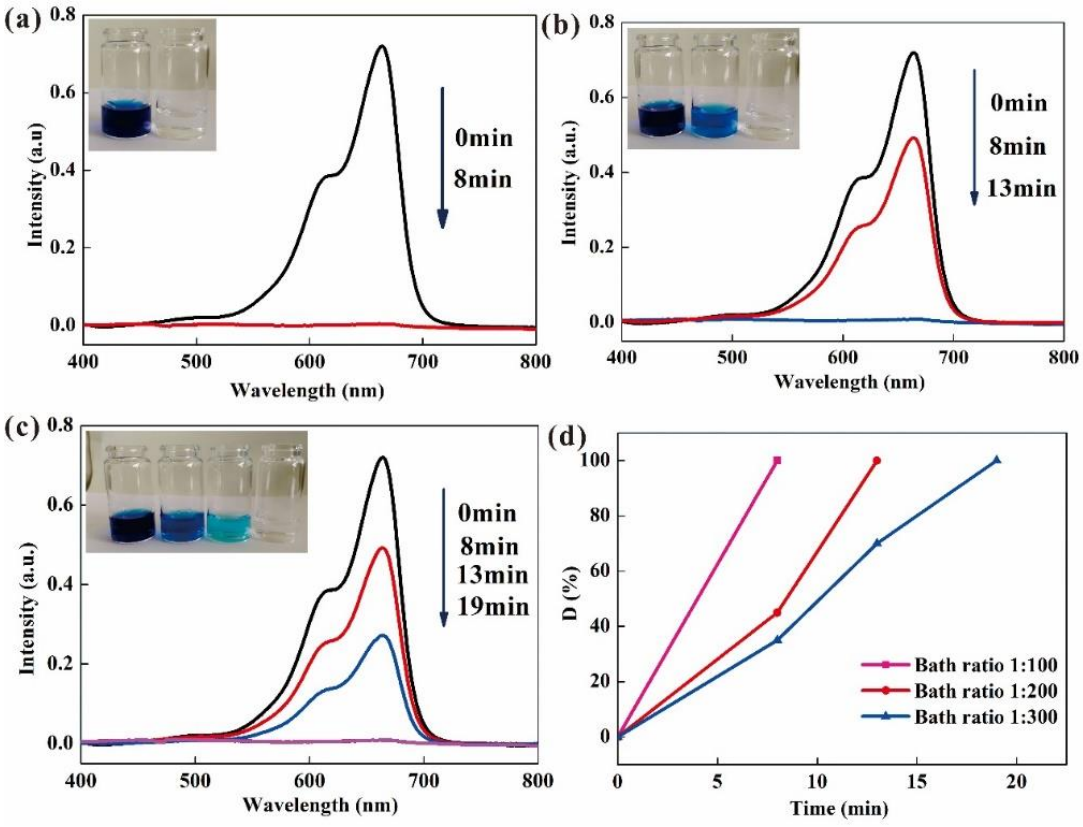

Fig. 3-3 Effect of bath ratio of Ag/GO nanoscroll composites to MB solution. (a) - (c) absorption spectra change for different bath ratios: (a) 1:100; (b) 1:200; (c) 1:300. (d) photodegradation rate of bath ratios. The suspension color changes are shown in the insets of (a) - (c). (conditions: initial MB concentration of 100 mg/L and UV light irradiation).

3.3.1.4 Effect of the light source

The mineralization rate under UV light (Fig. 3-4 (a)) was found to be nearly 40 times faster than under natural sunlight (Fig. 3-4 (b)). This indicates that Ag/GO nanoscroll composites have excellent photocatalytic properties under ultraviolet conditions. Fig. 3-4(c) exhibits that after 314 min of irradiation with natural sunlight, the photodegradation

rate reached 96%. Considering UV light accounts for 3 % - 5 % of the sun, we believe that the Ag/GO nanoscroll composites also have high photocatalytic activity under natural sunlight.

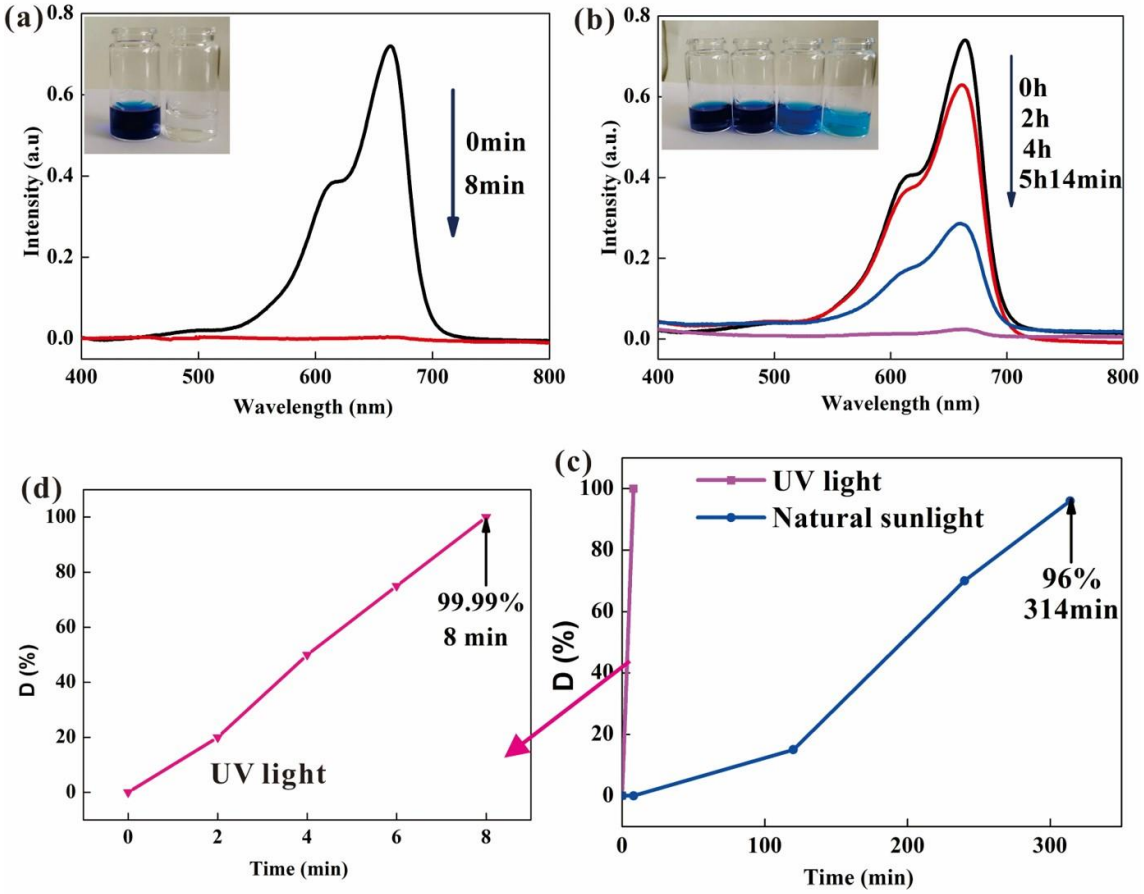

Fig. 3-4 Effect of the light source. (a) and (b) absorption spectra change for different light sources. (a) UV light; (b) natural sunlight. (c) photodegradation rates for different light sources. (d) magnification of UV light photodegradation curve. The suspension color changes are shown in the insets of (a) and (b). (conditions: bath ratio of Ag/GO nanoscroll composites to MB solution 1:100 and initial MB concentration of 100 mg/L).

Based on the above results, we concluded that the optimal photocatalytic conditions

for photodegradation are as follows: a bath ratio of Ag/GO nanoscroll composites to MB solution of 1: 100 with an initial MB concentration 100 mg/L exposed to UV light irradiation.

3.3.2 Photocatalytic reaction kinetics

The photodegradation reaction of MB by Ag/GO nanoscroll composites occurs via a pseudo-first-order reaction. The of plot of ln(C_0/C) against time is shown in Equation 3-10 [170, 171].

$$In\left(\frac{C_0}{C}\right) = kt \tag{3-10}$$

where, C_0 is the initial concentration of MB and C is the concentration of MB remaining at certain reaction time t. k is the apparent reaction rate constant, in term of min^{-1}. First-order kinetics of the Ag/GO nanoscroll composites is shown in Fig. 3-5. The pseudo first-order rate constants for the composites can be calculated as 0.0433 min^{-1}, as shown in the linear relationship.

As reported that the photocatalysis reaction kinetics occurs using the Langmuir-Hinshelwood mechanism [172]. Under the condition that the concentration of MB is low, the number of MB molecules is much less than generated hydroxyl radicals ($\cdot OH$) and superoxide radicals ($\cdot O_2^-$). As the number of oxidative radicals is constant, the reaction of the MB will not be very obvious. Therefore, the total reaction is simplified to mechanism for single molecule [173]. The model is shown in Equation 3-11.

$$r = \frac{kKC}{1+KC} \tag{3-11}$$

where C is the concentration of MB, k is the rate constant, K is the Langmuir constant.

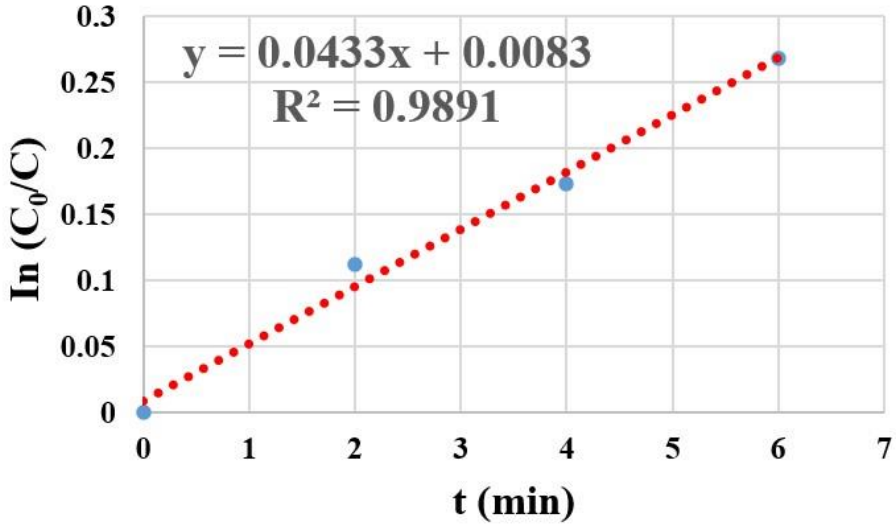

Fig. 3-5 The photocatalytic reaction kinetics of the Ag/GO nanoscroll composite photocatalyst.

3.3.3 Recyclability of the Ag/GO nanoscroll composite photocatalyst

Recyclability is an essential parameter for photocatalysts in practical applications. To determine the reusability of the Ag/GO nanoscroll composites, ten consecutive cycles were carried out under the optimal conditions discussed above. Fig. 3-6 shows the ten successive photodegradation experiments. In each cycle, the Ag/GO nanoscroll composites completely mineralized MB to colorless within approximately 10 min. Compared with other reported photocatalysts (Table 3-1), the Ag/GO nanoscroll composites exhibit a higher photodegradation rate within less time after multiple cycles. This result shows that the nanoscroll composites can be reused for photodegradation. This is because the AgNPs absorb the UV light to activate electrons with no other physical or chemical reaction required; therefore, the catalyst is not consumed during the total photodegradation. When there is no light, the AgNPs return to the Ag/GO nanoscroll composites with no change to their original state. In addition, the nanoscrolls provide

sufficient space to prevent the AgNPs from oxidizing and aggregating, which allows the AgNPs to be reused for numerous photodegradation cycles.

To confirm the Ag/GO nanoscroll composites can be reused without exhibiting loss, EDS and XRD were carried out before and after ten photodegradation cycles, as shown in Fig. 3-7. The EDS analysis shows that the main elements of the Ag/GO nanoscroll composites are C, O, and Ag (Fig. 3-7 (a) - (b)). The atom ratios of C, O, and Ag change from 42.96 %, 22.35 %, and 34.96 %, respectively, to 44.17 %, 22.41 %, and 31.42 %, demonstrating that the composition of the Ag/GO nanoscroll composites remains stable. As shown in Fig. 3-7 (c), after ten cycles, the sharp peaks of the composites diffraction pattern show no differences to those in the zero-cycle pattern, which is consistent with the result of EDS analysis.

FT-IR analysis (Fig. 3-7 (d)) of the decolorized solution was carried out to show that the MB organic matter had degraded. Characteristic peaks were detected at 1610 cm^{-1} and 3350 cm^{-1}, which corresponds to the peaks of water (H_2O) in the infrared spectrum. The result shows that after photocatalysis, the organic MB molecules were degraded to inorganic matter. This further indicates that the Ag/GO nanoscroll composites can be effectively used for the photodegradation of dyes and can be reused numerous times.

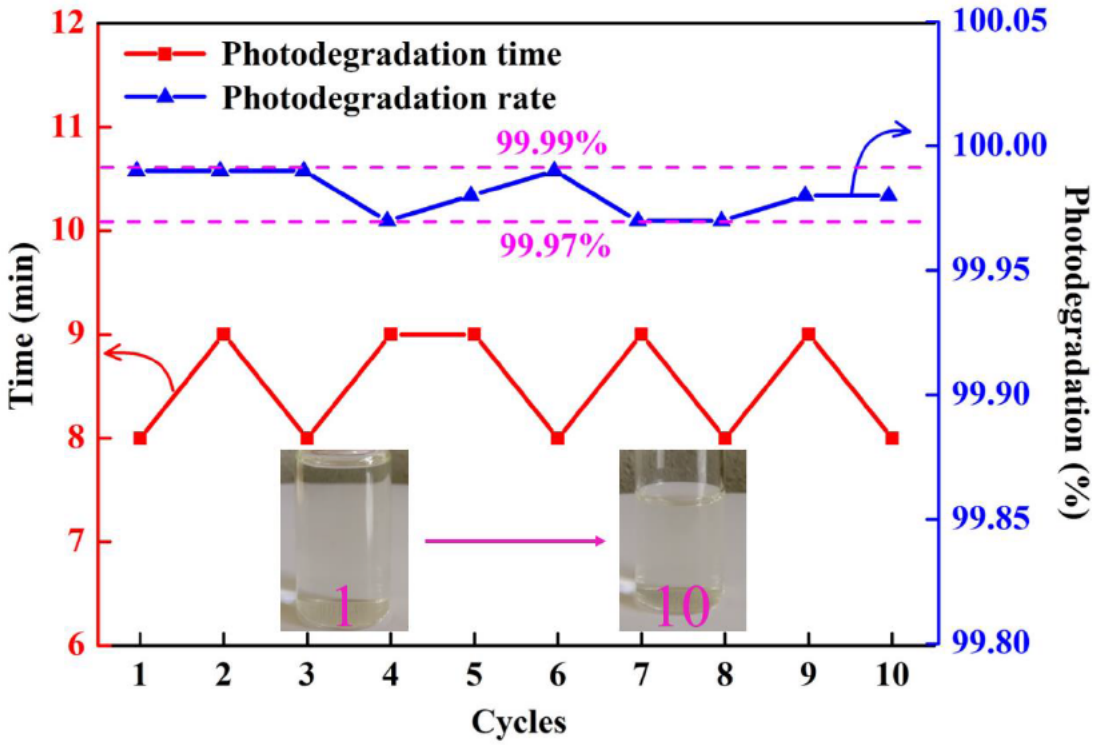

Fig. 3-6 Ten successive photodegradation experiments.

Table 3-1. Comparison of the Ag/GO nanoscroll composites with other composites reported for the photodegradation of dyes

Sample	Dye	Light source	Time of the last cycle	Cycle	Rate of the last cycle	Reference
RGO_5/TiO_2	MB	UV	60 min	3	65.6 %	[174]
CS-TiO_2 Nanohybrid	MB	UV	3 h	5	90 %	[175]
Hexagonal ZnO nanoplates	MB	UV	_	5	~ 90 %	[176]
ZnO@N-NpC composites	MB	UV	20 min	5	93 %	[177]
Ag/GO nanoscroll composites	MB	UV	8 min	10	99.98 %	This work

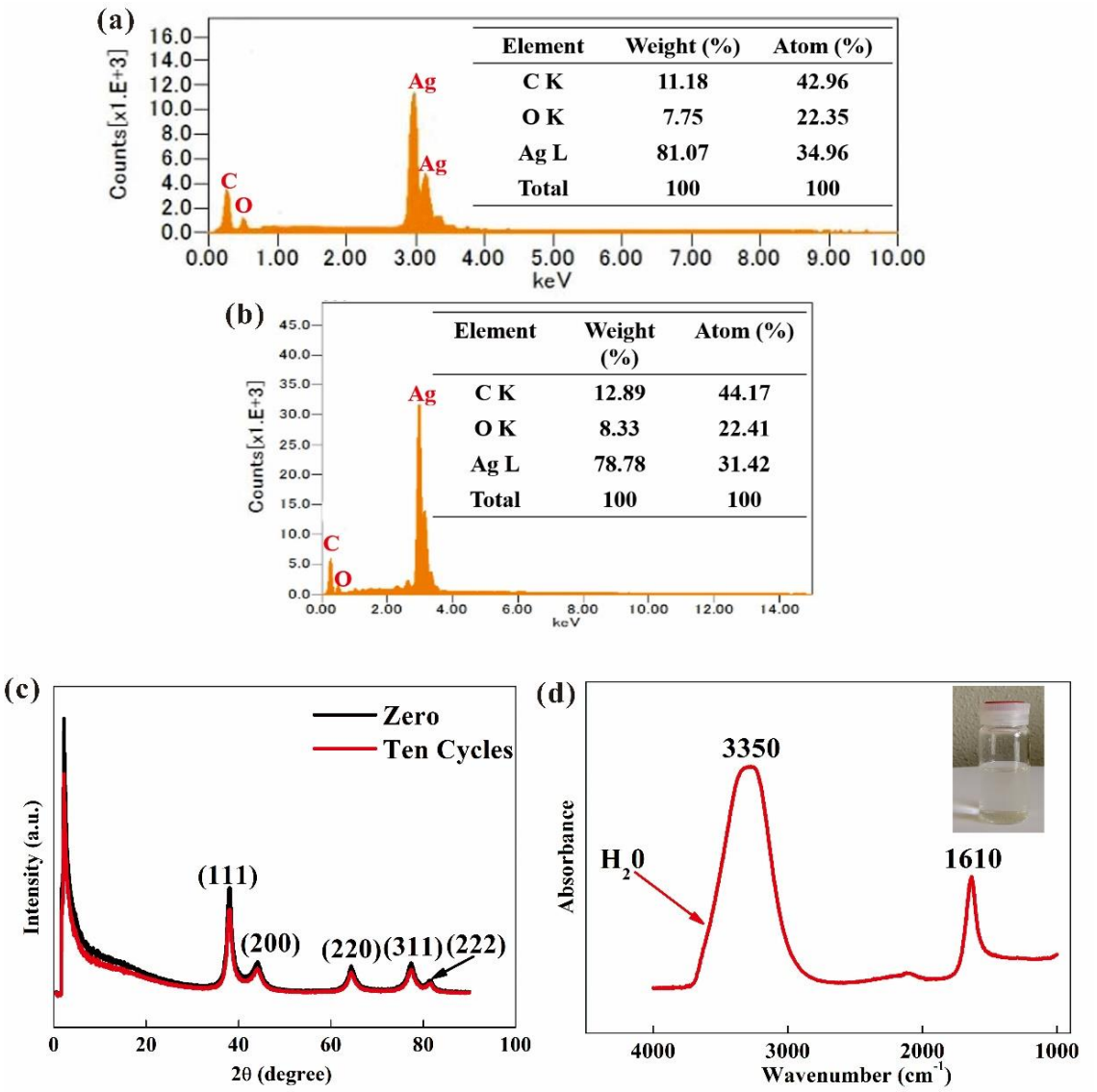

Fig. 3-7 Photocatalytic recyclability analysis of the Ag/GO nanoscroll composites. (a) EDS analysis of the Ag/GO nanoscroll composites before photodegradation. (b) EDS analysis of the Ag/GO nanoscroll composites after ten photodegradation cycles. (c) XRD patterns of the Ag/GO nanoscroll composites initially and following ten photodegradation cycles. (d) FT-IR analysis of the decolorized solution.

3.4 Conclusions

In conclusion, Ag/GO nanoscroll composites with a novel structure were synthesized for use as a recyclable photocatalyst. Ten consecutive cycles of MB mineralization were used to demonstrate the recyclable photocatalytic properties. The results show that under the optimal conditions (bath ratio of Ag/GO nanoscroll composites to MB of 1:100, initial MB concentration of 100 mg/L, and UV light irradiation), the nanoscroll composites can mineralize MB to colorless within 10 min in all cycles, and no loss was exhibited after ten cycles. This performance is attributed to the open-ended nanoscroll structures, which provide not only enough space for the AgNPs to prevent aggregation and oxidization, but also abundant pathways for AgNPs to transfer during photodegradation. We anticipate that the Ag/GO nanoscroll composites synthesized in this chapter can be used as a recyclable photocatalyst in photocatalytic materials.

Chapter 4

Synthesis and antioxidant stability of "sandwich" copper nanoparticle @ graphene oxide composites

Chapter 4: Synthesis and antioxidant stability of "sandwich" copper nanoparticle @ graphene oxide composites

4.1 Introduction

Metal nanoparticles have attracted significant attention in the field of nanoscale science for decades because of their unique chemical, physical, electronic, and magnetic properties, as well as their catalytic activity and potential for sensory and optical applications. [178-183]. Based on these unusual properties, metal nanoparticles can be used as catalysts or components in electronic devices, chemical and biological sensors, and photonic devices [184-187]. Among all metal nanoparticles, copper nanoparticles (CuNPs) have garnered particular interest due to their high electrical conductivity, catalytic performance, and antibacterial ability [188-192]. Additionally, the production cost of CuNPs is generally much lower than that of noble nanoparticles [193, 194]. Nia et al. reported the electrochemical deposition of copper nanoparticles on reduced graphene oxide using a facile one-step method and showed that the product can be used as a nonenzymatic hydrogen peroxide sensor [192]. Similarly, Menna et al. prepared graphene-stabilized zero-valent copper nanoparticles use in photocatalytic water splitting [195]. Simon et al. described a synthesis for copper nanocluster-doped HAP NPs which act as nanocarriers for antibacterial drug delivery [196]. However, it is highly challenging to maintain CuNPs in metallic form because bare CuNPs are readily oxidized to form

Cu_2O and CuO when exposed to air under ambient conditions [197, 198]. Therefore, there exists an urgent need to generate CuNPs that demonstrate enhanced antioxidant stability both in air and at high temperatures.

Several strategies have been directed towards achieving antioxidant stability for CuNPs, including introducing polymer coatings [199, 200], metallic coats[201, 202], or carbon material carriers [203, 204]. Because of the relatively high costs and the charge transport properties of coatings [205], the implementation of a graphene carrier represents one of the most suitable options for the deposition of CuNPs. Wang et al. synthesized the copper nanoparticles encapsulated by multi-layer graphene exhibited a high degree of thermal stability [206]. Guo et al. also prepared copper nanoparticles on graphene support [207], and Jin et al. generated Cu/graphene that showed high catalytic activity [208]. However, the mechanism of graphene formed on CuNPs is governed by the adsorption-diffusion method. For example, passivating the surface of CuNPs with a single-layered C atom hinders the formation of multi-layered graphene [209]. The resulting single-layered graphene is not sufficient to protect CuNPs from oxidation. Furthermore, the formation temperature of graphene-coated CuNPs is very high, which can be dangerous and is also not environmentally friendly [200] [208].

In this chapter, we describe the synthesis of stable CuNPs intercalated into graphene oxide composites (CuNPs@GO composites). These materials are fabricated at room temperature using an in-situ liquid-phase reduction method. The intercalation process forms a sandwich structure, wherein the GO sheets are served as the carriers and stabilizers for CuNPs by covering them to prevent their oxidation. The large surface area

of GO layer provides enough space for CuNPs while protecting them from aggregation. To confirm that the sandwich structure can effectively prevent oxidation of CuNPs, the air stability, high-temperature stability, and conductivity of the CuNPs@GO composites were carried out. The analysis based on TEM, XRD and Raman techniques shows that the synthesized composites exhibit enhanced antioxidant stability and conductivity both in air and at high temperatures.

4.2 Experimental

4.2.1 Materials and reagents

The reagents, H_2SO_4, $KMnO_4$, H_2O_2, HCl, $CuSO_4 \cdot 5H_2O$, L-ascorbic acid ($C_6H_8O_6$), and 2-Dimethylethanolamine (DMEA), were all provided by Wako Pure Chemical Industries Ltd., Japan. Graphite flakes (median 7-10 microns) were obtained from Alfa Aesar, a Johnson Matthey Co., Ltd., Japan. All chemicals were analytical grade reagents and used without further treatment. Deionized water was used throughout these investigations.

4.2.2 Synthesis of CuNPs@GO composites

GO was synthesized from graphite flakes using a modified version of the Hummers method [118]. The CuNPs@GO composites were synthesized via the following in-situ liquid-phase reduction method. An aqueous solution of GO (5 %, 20 mL) was stirred (600 rpm/min) for 30 min at room temperature. Then, $CuSO_4 \cdot 5H_2O$ (0.75 g) was added, followed by the addition of DMEA (0.254 mL). After all reagents were dissolved, the L-

ascorbic acid solution (26.4 mg/mL) was added dropwise. The mixture was then stirred for four hours at room temperature. The CuNPs located on the surface of the GO sheets were removed by sonication. Finally, the mixture was washed twice by deionized water, separated by centrifugation (5000 rpm, 10 min) to remove impurities, and re-dispersed in deionized water to obtain the composites comprised of copper nanoparticles intercalated in graphene oxide.

4.2.3 Antioxidant stability testing

4.2.3.1 Air stability testing

The synthesized CuNPs@GO composites were dried using a vacuum freeze dryer, and then exposed to air for 21 weeks.

4.2.3.2 High-temperature stability testing

CuNPs@GO composite membranes (30 mm × 20 mm × 0.5 μm) were formed on polyimide films using a simple solution casting method. Then, the developed composite membranes were heated at different temperatures (50 °C, 90 °C, 110 °C, and 100 °C) for 30 min with a thermo-compressor (F = 0 N). Immediately following the heating process, the membranes were rapidly returned to room temperature for analysis. Fig. 4-1 displays the high-temperature analysis heating process.

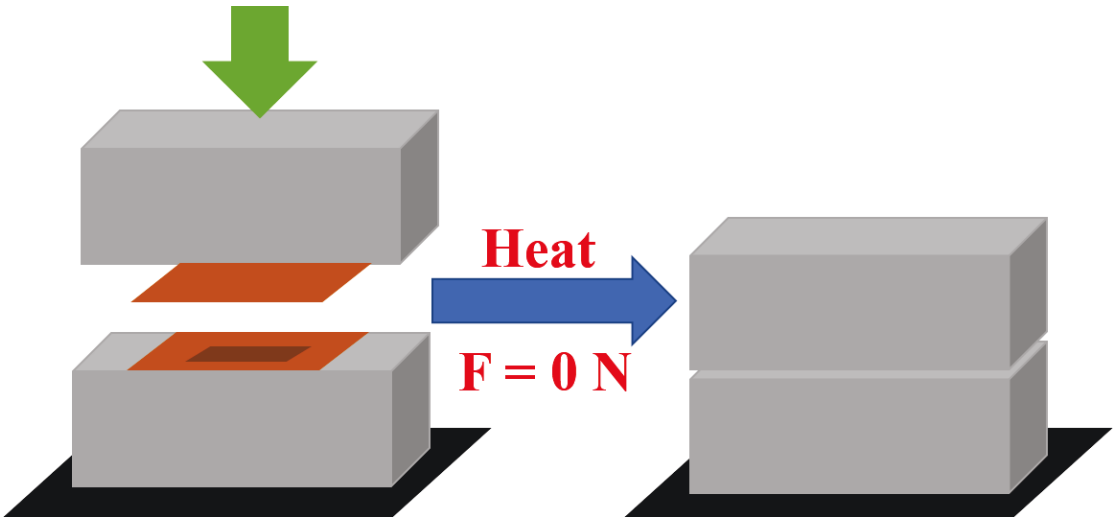

Fig. 4-1 The process of heating

4.2.3.3 Conductivity testing

The conductivity of synthesized composites was tested using four-point Probe method by a high resistivity meter (MCP - HT450, JP) (Fig. 4-2). The samples used were the same as the high-temperature stability testing. The four probes are arranged in a straight line and the voltage is applied to the sample surface. The current of probes 1 and 4 is I, the voltage of probes 2 and 3 is V, and the distance between the probes is L_1, L_2 and L_3, the conductivity is as follows:

$$\sigma = \frac{I}{2\pi V}\left(\frac{1}{L_1} + \frac{1}{L_3} - \frac{1}{L_1+L_2} - \frac{1}{L_2+L_3}\right) \quad (4\text{-}1)$$

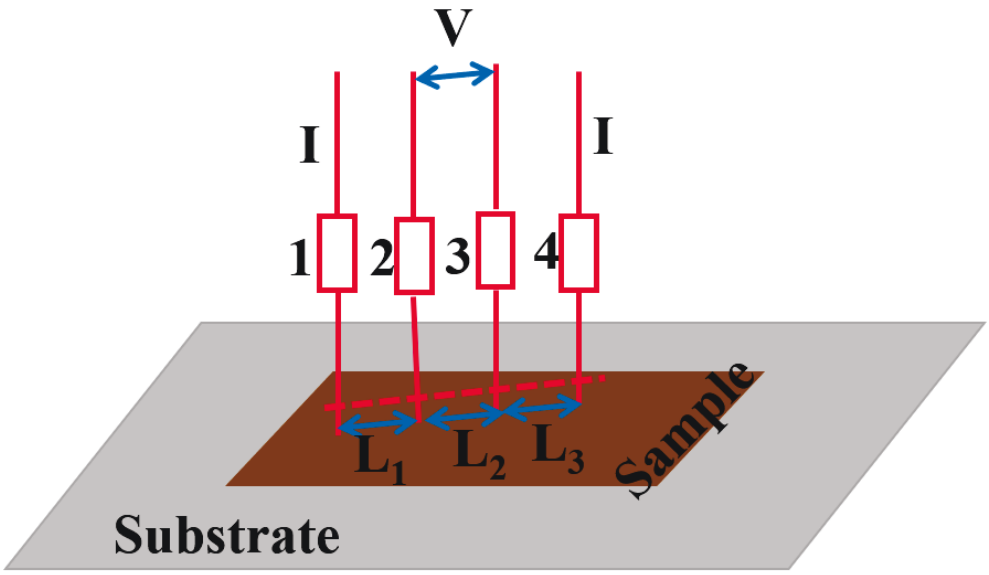

Fig. 4-2 The conductivity testing of CuNPs@GO composites

4.2.4 Instruments and characterizations

The CuNPs@GO composites were dried before taking morphological measurements and conducting analytical characterization.

4.2.4.1 Observations related to composite morphologies

Transmission electron microscopy (TEM) was conducted to examine the nanostructure of the CuNPs@GO composites. The images were obtained using a JEOL JEM 2010 TEM instrument, operating at 200kV. The distribution mapping of elements was conducted using an energy dispersive spectroscopy (EDS; S3000 N, Hitachi, Japan).

4.2.4.2 XRD analysis

X-ray diffraction (XRD) measurements were performed on a MiniFlex 300 XRD instrument using Cu Kα radiation. The CuNPs@GO composites were prepared as pressed

powder samples stuck to carbon tape and then attached to the scanning sample stage. The diffraction pattern was obtained at diffraction angles between 2θ = 5 - 85° at a scanning speed of 4° min^{-1} with a 0.02° divergence slit size. The samples (exposed to air for 21 weeks and heated to different temperatures) were re-examined XRD.

4.2.4.3 Raman analysis

Raman spectra were taken using a Raman RXN system spectroscopy instrument (Hololab 5000). The 532 nm laser was used as the excitation source. The scanning range spanned 500 to 2500 cm^{-1}. Samples were tested in solution.

4.2.4.4 Thermogravimetric analysis (TGA)

The thermal analysis of CuNPs@GO composites was conducted using a thermogravimetric analyzer (TG - DTA, TG 8120, Rigaku, Japan). The CuNPs@GO composite powder (3 - 6 mg) was collected in a standard aluminum (Al) crucible and scanned at a heating rate of 10 °C/min over the temperature range 30 - 650 °C under nitrogen flow. The derivative of TGA (the DTG) was calculated using the central finite difference method shown in Equation 4-2. where Δt is the time interval for reading the residual sample weight [210], and $W_{t+\Delta t} - W_{t-\Delta t}$ is the residual weight of the sample at time t + Δt and t - Δt, respectively [211].

$$\mathrm{DTG} = \frac{W_{t+\Delta t} - W_{t-\Delta t}}{2\Delta t} \quad (4\text{-}2)$$

The times associated with each weight loss and the maximum decomposition temperature (T_{max}) of the CuNPs@GO composites were calculated from the DTG curve [212].

4.3 Results and discussion

4.3.1 Characterization of the CuNPs@GO composites

Most reported chemical reduction methods rely on organic solvents and environmentally hazardous reducing agents [213-215]. Conversely, this work employs the L-ascorbic acid as an ecologically friendly reducing agent. The L-ascorbic acid is highly polar, and the electrons in the lactone ring carbonyl double bond, double bonds, and the hydroxyl group lone pair can form a conjugated system [216]. The "semi-dehydroascorbic acid" and then the dehydroascorbic acid is produced following dehydrogenation of the L-ascorbic acid (Fig. 4-3). The L-ascorbic acid and dehydroascorbic acid then constitute the redox system for the reduction process. Meanwhile, the lone pairs of electrons (e^-) in the polar groups of L-ascorbic acid can occupy two sp orbitals of Cu^{2+}, which leads to the successful reduction of Cu^{2+} to Cu^0 nanoparticles [216]. The overall reduction process is shown in Fig. 4-3, and Equation 4-3 and 4-4 show the redox reactions taking place [216, 217].

$$C_6H_8O_6 \rightarrow C_6H_6O_6 + 2H^+ + 2e^- \quad (4\text{-}3)$$

$$Cu^{2+} + 2e^- \rightarrow Cu^0 \quad (4\text{-}4)$$

Because of these interactions, the nanosized CuNPs are easily synthesized between the GO sheets and form sandwich structures. It is observed from the TEM image in Fig. 4-4 (a) that the CuNPs are uniformly located between the GO sheets, which allows verification of their target sandwich structure morphology. Fig. 4-4 (b) displays the TEM image of the isolated CuNPs, which shows that the average diameter of the CuNPs is 10 nm. This is a result of the limited distance between GO sheets, which efficiently controls

the growth of the CuNPs during reduction. The measured d-spacing values of the CuNPs lattice are 2.1 Å, which corresponds to the (111) lattice plane of Cu^0 (Fig. 4-4 (b), inset) [208, 218]. This is further evidence that the Cu^{2+} was reduced to Cu^0 nanoparticles by L-ascorbic acid, as described above and illustrated in Fig. 4-3. The EDS area mapping results (Fig. 4-4 (c-e)) were analyzed to investigate the homogeneity of the component elements. We determined that there are a high density and even distribution of CuNPs within the CuNPs@GO composites.

Fig. 4-4 (f) shows the XRD diffractograms of GO and CuNPs@GO composites. According to the Bragg Formula ($2d \sin\theta = n\lambda$), the sharp peak at 2θ = 2.22° corresponds to the interlayer distance of the GO sheets (001) [219]. The sharp peak of GO (001) is conserved and unchanged in the CuNPs@GO composites curve. This observation supports the conclusion that GO is used as the carrier and stabilizer for the CuNPs in the composite structures without undergoing any chemical reaction throughout the in-situ liquid-phase reduction process. Three high-intensity diffraction peaks located at 2θ = 43.42°, 50.56°, and 74.16° correspond to the three crystalline planes (111), (200), and (220) of the CuNPs face-centered cubic structure (JCPDS: 04-0836; a = 0.3615 nm) [220, 221], respectively. This XRD result provides further evidence that the CuNPs were successfully reduced.

To confirm the CuNPs reduction reaction, the Raman spectra of GO and CuNPs@GO composites were acquired, these are compared in Fig. 4-4 (g). both a D band and a G band are present in all poly-aromatic hydrocarbons[222], and these bands are directly related to the “molecular” picture of carbon materials[223]. The D band peak at 1200 - 1400 cm^-

^{1} originates from the breathing modes of sp^2 hybridized atoms in the carbon ring of networks. Therefore, this band is considered the peak of disordered vibration [224]. Similarly, the G band peak around 1600 cm^{-1} arises from the stretching motion of all pairs of sp^2 hybridized atoms in chains and rings, so it is considered the ordered vibration peak [225]. Based on the analysis of Fig. 4-4 (g), the difference between the D and G band peak of GO and CuNPs@GO composites are clearly observed. The intensity ratio of the D band to the G band (I_D/I_G) for GO is 0.98, while the I_D/I_G for CuNPs@GO composites is 0.79. This difference is likely due to the presence of CuNPs. Additionally, some defects in the GO could be repaired, resulting in a reduction of the intensity ratio. The formation of these Raman peaks is a result of vibrations of molecules or covalent bonds. Therefore, no peaks correspond to CuNPs in the Raman spectra because the CuNPs only contain metal-metal bonds. The results of the Raman analysis are consistent with the conclusions based on the XRD.

In short, characterization of the CuNPs@GO composites using various techniques confirmed that the sandwich structured composites were successfully synthesized with nanosized CuNPs intercalated between the sheets of GO.

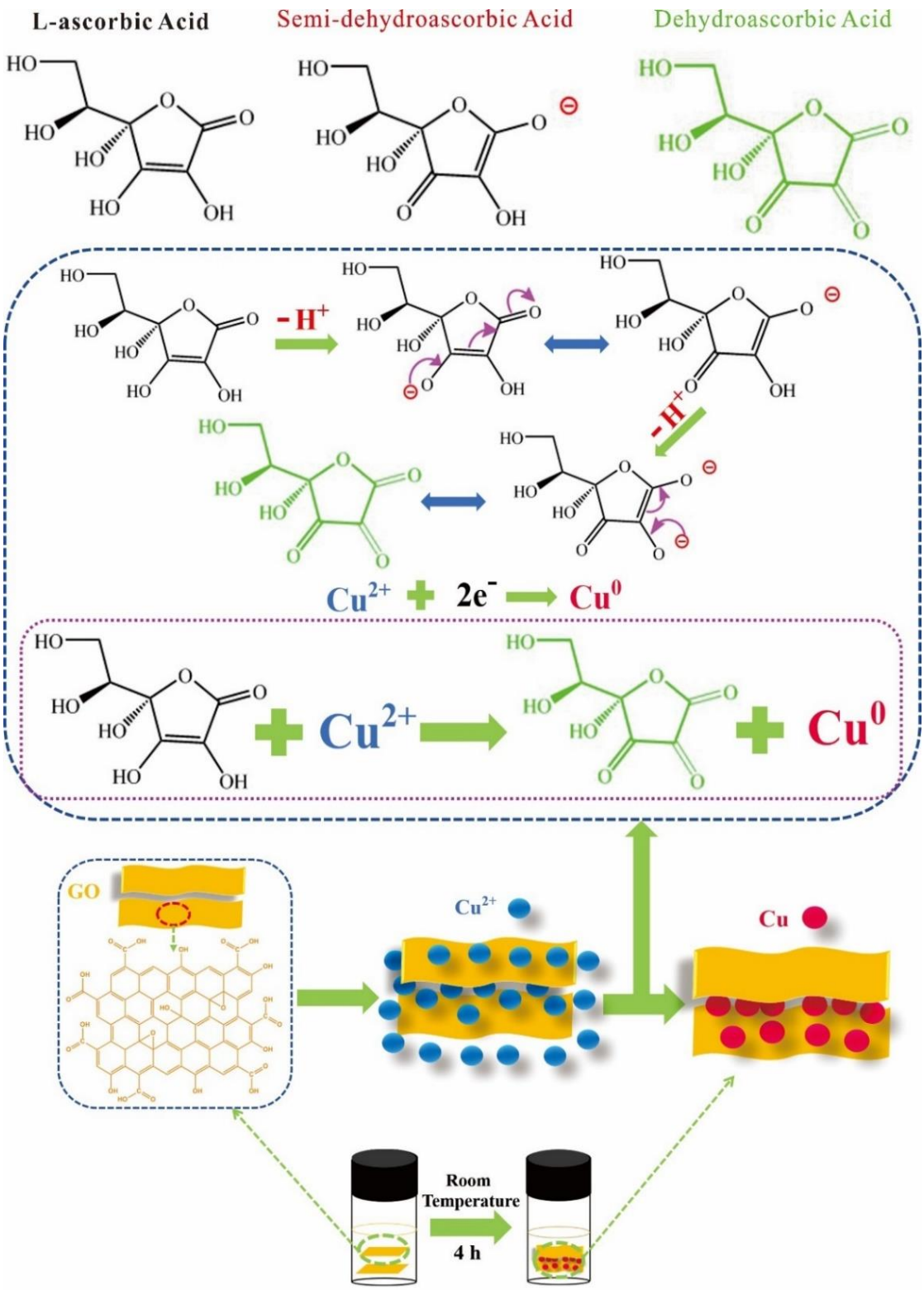

Fig. 4-3 Schematic showing the CuNPs@GO composites' reduction reaction process.

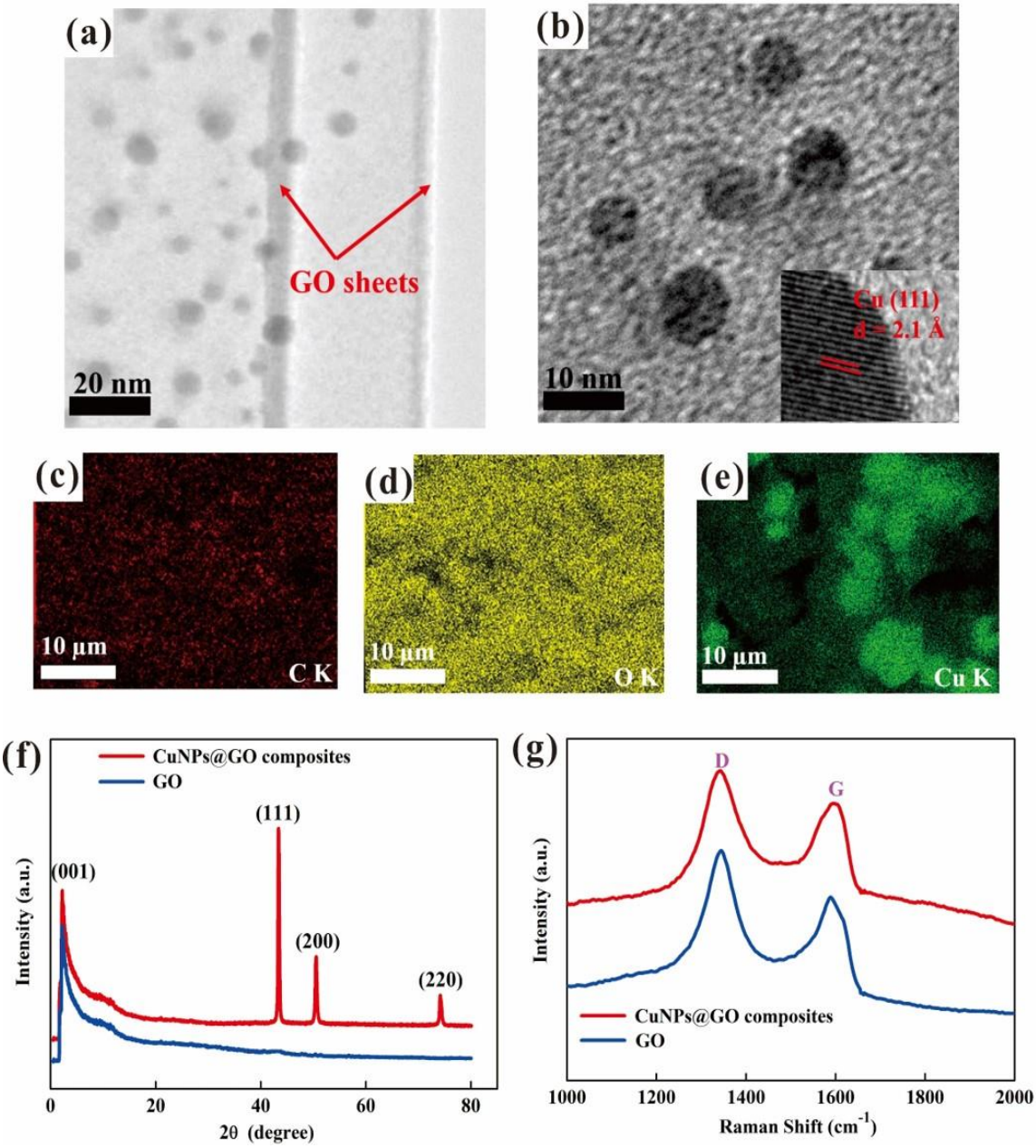

Fig. 4-4 Characterization of the synthesized CuNPs@GO composites. (a) TEM image of CuNPs@GO composites; (b) TEM image of CuNPs; (c-e) EDS mapping of CuNPs@GO composites: (c) C, (d) O, (e) Cu; (f) XRD diffractograms of GO and CuNPs@GO composites; (g) Raman spectra of GO and CuNPs@GO composites.

4.3.2 Analysis of antioxidant stability

The antioxidant stability of CuNPs is a significant property to consider when

determining their potential practical applications. Therefore, the air stability and the high-temperature stability of the synthesized CuNPs@GO composites were evaluated to confirm that the sandwich structure obtained in this chapter promotes enhanced stability against oxidation.

4.3.2.1 Air stability

The air stability of the synthesized composites was tested by drying them and then exposing them to air for 21 weeks under ambient conditions. The XRD and Raman analyses of the CuNPs@GO composites were conducted before and after exposure to air. The XRD spectra collected for the composites before and after the air stability test are shown in Fig. 4-5 (a). It is clear from these spectra that the crystallinity of CuNPs has no changed following exposure to air for 21 weeks. In addition, oxidation of the CuNPs@GO composites would result in Cu-O bond formation; however, no covalent bond peaks are observed in the Raman spectra (Fig. 4-5 (b)) after 21 weeks, compared with the curve at 0 weeks. Therefore, the results of both XRD and Raman analysis verify that the sandwich structure can efficiently protect CuNPs from oxidation following exposure to air under ambient conditions.

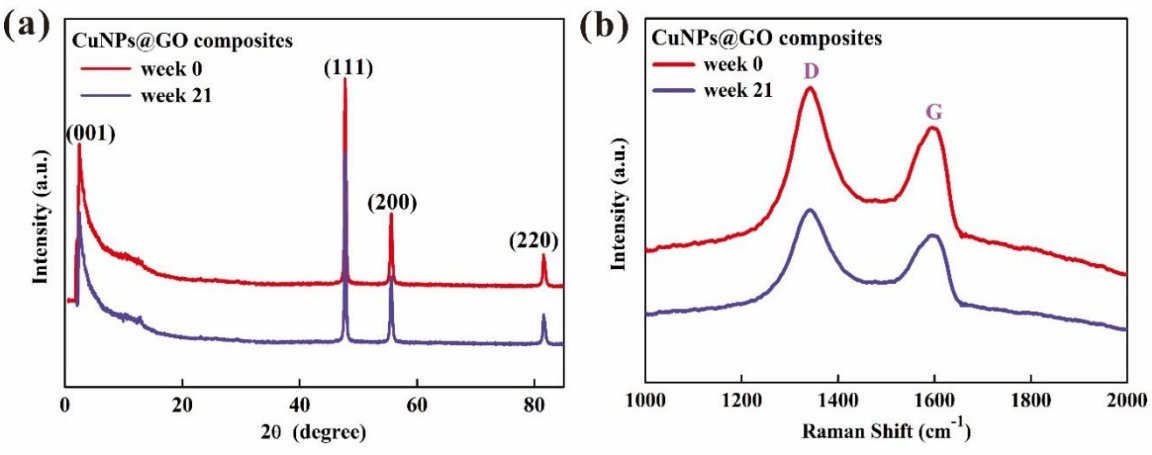

Fig. 4-5 (a) XRD spectra of CuNPs@GO composites at week 0 and week 21; (b) Raman spectra of CuNPs@GO composite at week 0 and week 21.

4.3.2.2 High-temperature stability

To assess the high temperature stability of CuNPs@GO composites, composite membranes were generated on the polyimide film using a solution casting method. Different temperature conditions (50 °C, 90 °C, 110 °C, and 100 °C) were tested using thermo-compressor (F = 0 N).

Analysis of TGA and DTG curves was conducted to quantify the weight change and thermal decomposition of the CuNPs@GO composites. As shown in Fig. 4-6 (a), the thermal degradation of the CuNPs@GO composites occurs in four steps. The details of the weight loss conditions at each temperature point are listed in Table 4-1. The first weight loss step is consistent with the first endothermic peak of the DTG curve at 70.65 °C, and this step represents the evaporation of the physisorbed water [193]. The second stage corresponds to the loss of bound water (from hydroxyl and carboxyl units), and the third weight loss step is due to the degradation of the polymeric backbone of the GO. The final endothermic degradation has the fastest degradation speed (T_P = 3.84 %/min) and the most

significant weight loss, and this stage represents the loss of CuNPs. The degradation of the CuNPs occurs at the last stage because of the sandwich structure. Specifically, the cover of the GO sheets initially protects the CuNPs from degradation, once the GO is degraded, the CuNPs are exposed and vulnerable to degradation with the rising temperature. The total weight loss experienced by the CuNPs@GO composites is equivalent to 58.95%, so the TGA data demonstrate that the CuNPs@GO composites have good thermal stability.

Fig. 4-6 (b) shows the XRD spectra of the CuNPs@GO composite membranes at RT, and heated to 50 °C, 90 °C, and 110 °C. The spectra show that when the composite membranes are heated to a temperature up to and including 90 °C, the CuNPs@GO composites exhibit high antioxidant ability; however, the temperature is increased to 110 °C, the GO is reduced and the CuNPs are oxidized. To determine the specific temperature at which CuNPs@GO composites oxidation occurs, the additional heating temperature of 100 °C was tested, as shown in Fig. 4-6 (c). All XRD patterns are clearly observed in the spectra, including the (111), (200), and (220) crystal lattice planes of CuNPs, the (110) and (222) crystal lattice planes of Cu_2O (JCPSD: 05-0667) [221], and the (200) and (022) of the crystal lattice planes of CuO (JCPSD: 89-8531) [226]. All of these structures are detected because two oxidation steps occur as the temperature rises. The first product is Cu_2O, which forms at a lower temperature, and CuO is formed at higher temperatures. These processes are described by reaction Equations 4-5 and 4-6 [227].

$$4Cu + O_2 \rightarrow 2Cu_2O \quad (4\text{-}5)$$

$$2Cu_2O + O_2 \rightarrow 4CuO \quad (4\text{-}6)$$

Based on the XRD results presented, the CuNPs@GO composites are oxidized at around 100 °C. Additionally, the diffraction peak that appeared at $2\theta = 20.5°$ on the XRD spectrum (Fig. 4-6 (c)) corresponds to the (200) plane of reduced GO, which indicates that the GO was reduced at 100 °C.

In summary, the CuNPs@GO composites remain stable at temperatures up to 90 °C, which confirms that the synthesized sandwich composites exhibit high-temperature stability.

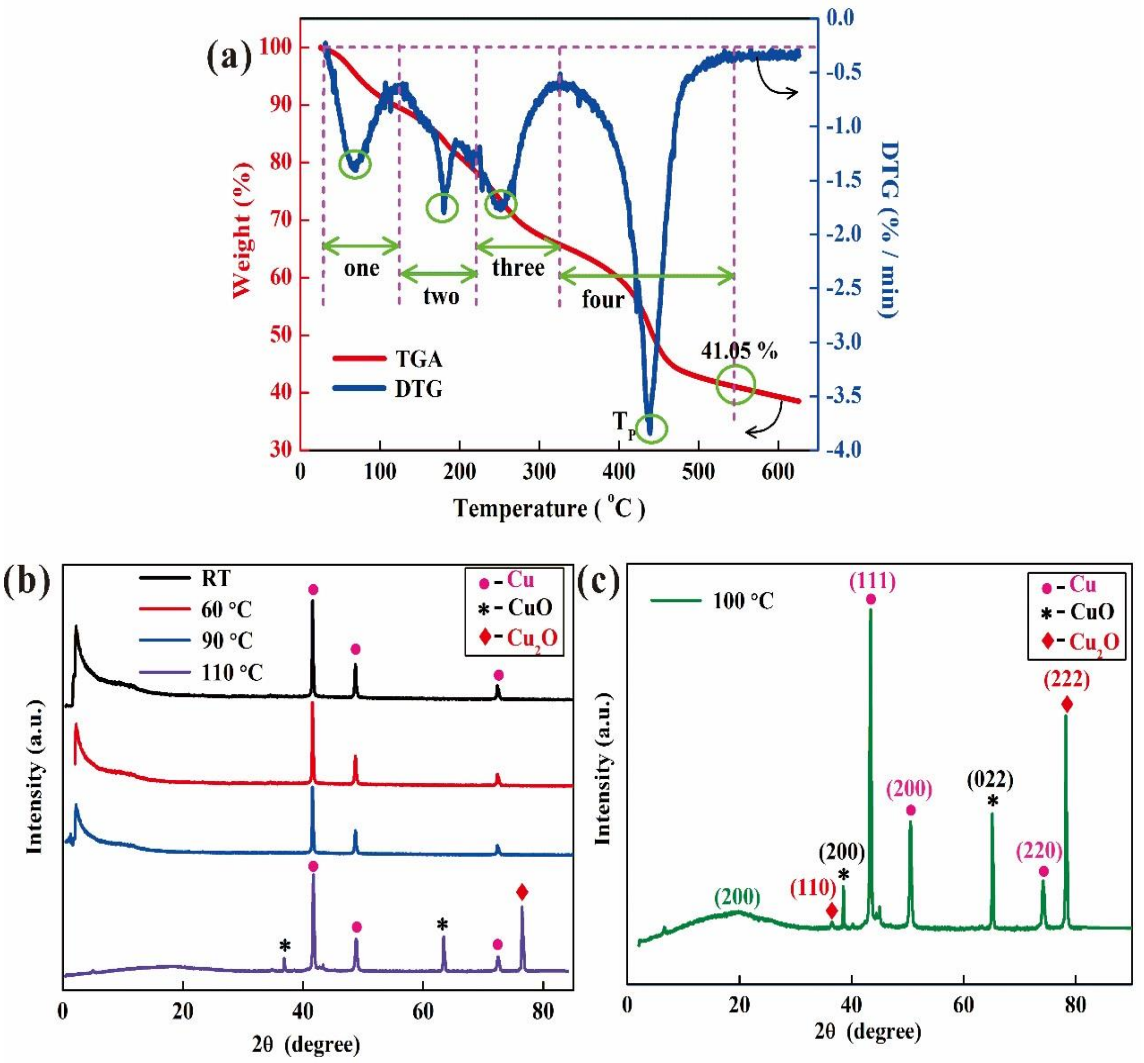

Fig. 4-6 Analysis of the thermal stability of CuNPs@GO composites. (a) TGA and DTG curves; (b) XRD spectra of CuNPs@GO composites at room temperature (RT), 50 °C, 90 °C, and 110 °C; (c) XRD diffractogram of CuNPs@GO composites at 100 °C.

Table 4-1 CuNPs@GO composites' weight loss as a function of temperature.

Steps	Temperature (°C)	Weight (%)	Weight loss (%)	Speed (%/min)
One	70.65	89.51	10.49	1.36
Two	180.16	78.33	21.67	1.77
Three	252.05	65.72	34.28	1.73
Four (T_p)	438.75	41.05	58.95	3.84

4.3.2.3 The conductivity of CuNPs@GO composites

The conductivity result of the CuNPs@GO composites is shown in Table 4-2. The result shows that the composites' conductivity has barely changed (from 1.387×10^3 S/cm to 1.618×10^3 S/cm) after exposing to dry air for 21 weeks. However, heating the composites to 90 °C, the conductivity shows an obvious loss. This is because the amplitude of the CuNPs' lattice vibration increases, the scattering frequency increases as the temperature increases. As a result, the resistance was increased and the conductivity was decreased.

In short, the conductivity result of the synthesized composites shows no change after exposing to dry air for at least 21 weeks.

Table 4-2 The resistivity (Ω·cm) and conductivity (S/cm) results.

Count \ Sample	Week 0 Room temperature	Week 21 Room temperature	90 °C
Resistivity 1	7.425×10^{-4}	7.256×10^{-4}	3.044×10^{-2}
Resistivity 2	7.557×10^{-4}	3.290×10^{-4}	2.468×10^{-2}
Resistivity 3	7.232×10^{-4}	8.234×10^{-4}	2.786×10^{-3}
Resistivity 4	6.834×10^{-4}	8.256×10^{-4}	8.234×10^{-2}
Resistivity 5	8.012×10^{-4}	7.457×10^{-4}	8.121×10^{-2}
Resistivity 6	7.256×10^{-4}	7.897×10^{-4}	3.016×10^{-2}
Resistivity 7	7.347×10^{-4}	7.125×10^{-4}	2.246×10^{-3}
Resistivity 8	5.929×10^{-4}	6.258×10^{-4}	2.468×10^{-2}
Resistivity 9	6.914×10^{-4}	6.987×10^{-4}	3.859×10^{-2}
Resistivity 10	7.569×10^{-4}	7.278×10^{-4}	3.290×10^{-3}
Average	7.208×10^{-4}	6.178×10^{-4}	2.902×10^{-2}
Conductivity	1.387×10^{3}	1.618×10^{3}	3.445×10

4.4 Conclusions

CuNPs@GO composites were synthesized in high yield using an in-situ liquid-phase reduction method at room temperature. The intercalation process results in the formation of sandwich structures, where the CuNPs were located into the GO sheets. L-ascorbic acid was used as an eco-friendly reducing agent, and its strong polarity efficiently reduced Cu^{2+} to Cu^{0}. The limited interlayer distance of the GO sheets controlled the growth of CuNPs during the reducing process, such that they were uniformly generated with diameters of about 10 nm. To verify that the sandwich structure protected the CuNPs from oxidation, the CuNPs@GO composites' air stability and high-temperature stability were evaluated. The combined results of several analytical methods show that the CuNPs@GO composites exhibit no sign of oxidation after exposure to air for 21 weeks. Additionally, after heating the composites at temperatures up to 90 °C for 30 min, the CuNPs maintain their metallic nanoparticle form, and the GO is not reduced. Thus, it was confirmed that

the sandwich structured CuNPs@GO composites demonstrate excellent antioxidant stability both in ambient conditions and at high temperatures. In addition, the conductivity result of the synthesized composites shows no change after exposing to dry air for at least 21 weeks. These results indicate new potential research directions based on fabricating highly stable CuNPs.

Chapter 5

Overall conclusions

Chapter 5: Overall conclusions

This thesis was mainly devoted to studies on the fabrication of nanoparticle-based functional composites, and their properties and applications. Three kinds of shape-controlled, size-controlled nanocomposites were successfully fabricated, and their structural and functional properties were investigated and discussed in detail. The brief summaries are as follows:

Chapter 1 reviewed references and provided brief summaries of functional composites, including to nanomaterials, antibacterial materials, and photocatalytic materials.

In chapter 2, the Ag/GO nanoscroll composites were fabricated, and their antibacterial activity was investigated in detail. Three different molar ratios were carried out to study the optimal condition of the rolling up process. The result shows that when the $AgNO_3$ of 5.88 mmol was added into the GO solution of 42 mL at room temperature, the GO sheets were cut into pieces, Then, the Ag/GO nanoscroll composites with 100 nm in diameter are fabricated by the force of intermolecular hydrogen bonds, attached by lots of AgNPs (4 - 10 nm). The Ag/GO nanoscroll composites were proved to have long-lasting antibacterial activity. The result shows that after against the E. coli for 3 days, the inhibition rate of Ag/GO nanoscroll composites can still up to 99.99%. This is due to their open-ended tubular structures, and the composites provide abundant continuous channels and space to prevent the AgNPs from aggregating and oxidizing, which enhance the antibacterial activity of the composites to use for a long time.

In chapter 3, the photocatalytic application of Ag/GO nanoscroll composites was addressed. Ten consecutive cycles of MB mineralization were used to demonstrate the recyclable photocatalytic properties of synthesized nanoscroll composites. The results show that under the optimal conditions (bath ratio of Ag/GO nanoscroll composites to MB of 1:100, initial MB concentration of 100 mg/L, and UV light irradiation), the nanoscroll composites can mineralize MB to colorless within 10 min in all cycles, and no loss was exhibited after ten cycles. This performance is attributed to the open-ended nanoscroll structures, which provide not only enough space for the AgNPs to prevent aggregation and oxidization, but also abundant pathways for AgNPs to transfer during photodegradation.

In chapter 4, the fabrication and conductivity of CuNPs@GO composites were studied. The L-ascorbic acid was used as an eco-friendly reducing agent, and its strong polarity efficiently reduced Cu^{2+} to Cu^{0}. Owing to the limited interlayer distance of the GO sheets, controlled the growth of CuNPs during the reducing process, the CuNPs were uniformly generated with a diameter of about 10 nm. To verify that the sandwich structure protected the CuNPs from oxidation, the air stability and high- temperature stability of CuNPs@GO composites was evaluated. The combined results show that the CuNPs@GO composites exhibit no sign of oxidation after exposure to air for 21 weeks. Additionally, after heating the composites at temperatures up to 90 °C for 30 min, the CuNPs still maintain their metallic nanoparticle form, and the GO is not reduced. The conductivity result of the synthesized composites shows no change after exposure to dry air for at least 21 weeks. These results indicate new potential research directions based on fabricating

highly stable CuNPs with enhanced conductivity.

In summary, three types of nanoparticle-based composites have been successfully fabricated and their properties, structural analysis, and applications have been well discussed.

References

[1] S.J.R.J.R.S. Hasan, A review on nanoparticles: their synthesis and types, 2277 (2015) 2502.
[2] L.A. Kolahalam, I.V. Kasi Viswanath, B.S. Diwakar, B. Govindh, V. Reddy, Y.L.N. Murthy, Review on nanomaterials: Synthesis and applications, Materials Today: Proceedings 18 (2019) 2182-2190.
[3] K. Ganesh, D.J.A.J.A.D.D. Archana, Review Article on Targeted Polymeric Nanoparticles: An Overview, 3(3) (2013) 196-215.
[4] S.R. Mudshinge, A.B. Deore, S. Patil, C.M.J.S.p.j. Bhalgat, Nanoparticles: emerging carriers for drug delivery, 19(3) (2011) 129-141.
[5] N.C. Shinde, N.J. Keskar, P.D.J.R.J.P.B.C.S. Argade, Nanoparticles: Advances in drug delivery systems, 3 (2012) 922-929.
[6] R.M. Crooks, M. Zhao, L. Sun, V. Chechik, L.K.J.A.o.c.r. Yeung, Dendrimer-encapsulated metal nanoparticles: synthesis, characterization, and applications to catalysis, 34(3) (2001) 181-190.
[7] W.-T.J.J.o.b. Liu, bioengineering, Nanoparticles and their biological and environmental applications, 102(1) (2006) 1-7.
[8] M. Laad, V.K.S.J.J.o.K.S.U.-E.S. Jatti, Titanium oxide nanoparticles as additives in engine oil, 30(2) (2018) 116-122.
[9] D.R. Cooper, B. D'Anjou, N. Ghattamaneni, B. Harack, M. Hilke, A. Horth, N. Majlis, M. Massicotte, L. Vandsburger, E. Whiteway, V. Yu, Experimental Review of Graphene, ISRN Condensed Matter Physics 2012 (2012) 1-56.
[10] M.S. Dresselhaus, G. Dresselhaus, P. Eklund, A. Rao, Carbon nanotubes, The physics of fullerene-based and fullerene-related materials, Springer2000, pp. 331-379.
[11] N.J.J.o.m.r. Rodriguez, A review of catalytically grown carbon nanofibers, 8(12) (1993) 3233-3250.
[12] E. Hammel, X. Tang, M. Trampert, T. Schmitt, K. Mauthner, A. Eder, P.J.C. Pötschke, Carbon nanofibers for composite applications, 42(5-6) (2004) 1153-1158.
[13] N. Kumar, S. Kumbhat, Essentials in nanoscience and nanotechnology, (2016).
[14] K.S. Novoselov, A.K. Geim, S.V. Morozov, D. Jiang, Y. Zhang, S.V. Dubonos, I.V. Grigorieva, A.A.J.s. Firsov, Electric field effect in atomically thin carbon films, 306(5696) (2004) 666-669.
[15] X. Du, I. Skachko, A. Barker, E.Y.J.N.n. Andrei, Approaching ballistic transport in suspended graphene, 3(8) (2008) 491-495.
[16] C. Lee, X. Wei, J.W. Kysar, J.J.s. Hone, Measurement of the elastic properties and intrinsic strength of monolayer graphene, 321(5887) (2008) 385-388.

[17] A.A. Balandin, S. Ghosh, W. Bao, I. Calizo, D. Teweldebrhan, F. Miao, C.N.J.N.l. Lau, Superior thermal conductivity of single-layer graphene, 8(3) (2008) 902-907.
[18] H.J.S. Jiang, Chemical preparation of graphene-based nanomaterials and their applications in chemical and biological sensors, 7(17) (2011) 2413-2427.
[19] S. Yang, X. Feng, K.J.A.M. Müllen, Sandwich-like, graphene-based titania nanosheets with high surface area for fast lithium storage, 23(31) (2011) 3575-3579.
[20] Q. Xiang, J. Yu, M.J.J.o.t.A.C.S. Jaroniec, Synergetic effect of MoS2 and graphene as cocatalysts for enhanced photocatalytic H2 production activity of TiO2 nanoparticles, 134(15) (2012) 6575-6578.
[21] Y. Si, E.T.J.C.o.M. Samulski, Exfoliated graphene separated by platinum nanoparticles, 20(21) (2008) 6792-6797.
[22] C. Nethravathi, E. Anumol, M. Rajamathi, N.J.N. Ravishankar, Highly dispersed ultrafine Pt and PtRu nanoparticles on graphene: formation mechanism and electrocatalytic activity, 3(2) (2011) 569-571.
[23] N.J. Bell, Y.H. Ng, A. Du, H. Coster, S.C. Smith, R.J.T.J.o.P.C.C. Amal, Understanding the enhancement in photoelectrochemical properties of photocatalytically prepared TiO2-reduced graphene oxide composite, 115(13) (2011) 6004-6009.
[24] X. Huang, X. Zhou, L. Zhou, K. Qian, Y. Wang, Z. Liu, C.J.C. Yu, A facile one-step solvothermal synthesis of SnO2/graphene nanocomposite and its application as an anode material for lithium-ion batteries, 12(2) (2011) 278-281.
[25] H.Y. Koo, H.J. Lee, H.A. Go, Y.B. Lee, T.S. Bae, J.K. Kim, W.S.J.C.A.E.J. Choi, Graphene-Based Multifunctional Iron Oxide Nanosheets with Tunable Properties, 17(4) (2011) 1214-1219.
[26] M. Salavati-Niasari, F. Davar, N.J.P. Mir, Synthesis and characterization of metallic copper nanoparticles via thermal decomposition, 27(17) (2008) 3514-3518.
[27] S. Anu Mary Ealia, M.P. Saravanakumar, A review on the classification, characterisation, synthesis of nanoparticles and their application, IOP Conference Series: Materials Science and Engineering 263 (2017).
[28] E.J. Cho, H. Holback, K.C. Liu, S.A. Abouelmagd, J. Park, Y.J.M.p. Yeo, Nanoparticle characterization: state of the art, challenges, and emerging technologies, 10(6) (2013) 2093-2110.
[29] G. Franci, A. Falanga, S. Galdiero, L. Palomba, M. Rai, G. Morelli, M.J.M. Galdiero, Silver nanoparticles as potential antibacterial agents, 20(5) (2015) 8856-8874.
[30] S. Jana, T.J.J.o.N. Pal, Nanotechnology, Synthesis, characterization and catalytic application of silver nanoshell coated functionalized polystyrene beads, 7(6) (2007) 2151-2156.
[31] R. Stiufiuc, C. Iacovita, C.M. Lucaciu, G. Stiufiuc, A.G. Dutu, C. Braescu, N.J.N.r.l. Leopold, SERS-active silver colloids prepared by reduction of silver nitrate with short-chain polyethylene glycol, 8(1) (2013) 47.

[32] G.A. Evtugyn, R.V. Shamagsumova, P.V. Padnya, I.I. Stoikov, I.S.J.T. Antipin, Cholinesterase sensor based on glassy carbon electrode modified with Ag nanoparticles decorated with macrocyclic ligands, 127 (2014) 9-17.
[33] N.T. Thanh, L.A.J.N.T. Green, Functionalisation of nanoparticles for biomedical applications, 5(3) (2010) 213-230.
[34] N. Alon, Y. Miroshnikov, N. Perkas, I. Nissan, A. Gedanken, O.J.I.j.o.n. Shefi, Substrates coated with silver nanoparticles as a neuronal regenerative material, 9(Suppl 1) (2014) 23.
[35] Y. Luo, L. Ma, X. Zhang, A. Liang, Z.J.N.r.l. Jiang, SERS detection of dopamine using label-free acridine red as molecular probe in reduced graphene oxide/silver nanotriangle sol substrate, 10(1) (2015) 230.
[36] M. Bosetti, A. Massè, E. Tobin, M.J.B. Cannas, Silver coated materials for external fixation devices: in vitro biocompatibility and genotoxicity, 23(3) (2002) 887-892.
[37] P. Jain, T.J.B. Pradeep, bioengineering, Potential of silver nanoparticle-coated polyurethane foam as an antibacterial water filter, 90(1) (2005) 59-63.
[38] Q. Li, S. Mahendra, D.Y. Lyon, L. Brunet, M.V. Liga, D. Li, P.J.J.W.r. Alvarez, Antimicrobial nanomaterials for water disinfection and microbial control: potential applications and implications, 42(18) (2008) 4591-4602.
[39] L. Yang, F. Meng, X. Qu, L. Xia, F. Huang, S. Qin, M. Zhang, F. Xu, L. Sun, H. Liu, Multiple-twinned silver nanoparticles supported on mesoporous graphene with enhanced antibacterial activity, Carbon 155 (2019) 397-402.
[40] H. Huang, F. Yan, Y. Kek, C. Chew, G. Xu, W. Ji, P. Oh, S.J.L. Tang, Synthesis, characterization, and nonlinear optical properties of copper nanoparticles, 13(2) (1997) 172-175.
[41] K.J. Ziegler, R.C. Doty, K.P. Johnston, B.A. Korgel, Synthesis of Organic Monolayer-Stabilized Copper Nanocrystals in Supercritical Water, Journal of the American Chemical Society 123(32) (2001) 7797-7803.
[42] M.-S. Yeh, Y.-S. Yang, Y.-P. Lee, H.-F. Lee, Y.-H. Yeh, C.-S. Yeh, Formation and Characteristics of Cu Colloids from CuO Powder by Laser Irradiation in 2-Propanol, The Journal of Physical Chemistry B 103(33) (1999) 6851-6857.
[43] H. Wang, Y. Huang, Z. Tan, X. Hu, Fabrication and characterization of copper nanoparticle thin-films and the electrocatalytic behavior, Analytica Chimica Acta 526(1) (2004) 13-17.
[44] M.H. Kim, B. Lim, E.P. Lee, Y. Xia, Polyol synthesis of Cu2O nanoparticles: use of chloride to promote the formation of a cubic morphology, Journal of Materials Chemistry 18(34) (2008) 4069-4073.
[45] M. Salavati-Niasari, F. Davar, N. Mir, Synthesis and characterization of metallic copper nanoparticles via thermal decomposition, Polyhedron 27(17) (2008) 3514-3518.
[46] J.A. Eastman, S.U.S. Choi, S. Li, W. Yu, L.J. Thompson, Anomalously increased

effective thermal conductivities of ethylene glycol-based nanofluids containing copper nanoparticles, 78(6) (2001) 718-720.
[47] L. Lu, M.L. Sui, K. Lu, Cold rolling of bulk nanocrystalline copper, Acta Materialia 49(19) (2001) 4127-4134.
[48] N. Yang, J. Zhai, D. Wang, Y. Chen, L. Jiang, Two-Dimensional Graphene Bridges Enhanced Photoinduced Charge Transport in Dye-Sensitized Solar Cells, ACS Nano 4(2) (2010) 887-894.
[49] A. Ghorban Shiravizadeh, S.M. Elahi, S.A. Sebt, R. Yousefi, High performance of visible-NIR broad spectral photocurrent application of monodisperse PbSe nanocubes decorated on rGO sheets, Journal of Applied Physics 123(8) (2018) 083102.
[50] W.-P. Xu, L.-C. Zhang, J.-P. Li, Y. Lu, H.-H. Li, Y.-N. Ma, W.-D. Wang, S.-H. Yu, Facile synthesis of silver@graphene oxide nanocomposites and their enhanced antibacterial properties, Journal of Materials Chemistry 21(12) (2011) 4593-4597.
[51] Y. Raghupathy, A. Kamboj, M.Y. Rekha, N.P. Narasimha Rao, C. Srivastava, Copper-graphene oxide composite coatings for corrosion protection of mild steel in 3.5% NaCl, Thin Solid Films 636 (2017) 107-115.
[52] C. Basavaraja, W.J. Kim, Y.D. Kim, D.S. Huh, Synthesis of polyaniline-gold/graphene oxide composite and microwave absorption characteristics of the composite films, Materials Letters 65(19) (2011) 3120-3123.
[53] R.G. Chaudhary, A.K. Potbhare, S.K.T. Aziz, M.S. Umekar, S.S. Bhuyar, A. Mondal, Phytochemically fabricated reduced graphene Oxide-ZnO NCs by Sesbania bispinosa for photocatalytic performances, Materials Today: Proceedings (2020).
[54] M.W. Kadi, A.A. Ismail, R.M. Mohamed, D.W. Bahnemann, Photodegradation of the herbicide imazapyr over mesoporous In2O3-TiO2 nanocomposites with enhanced photonic efficiency, Separation and Purification Technology 205 (2018) 66-73.
[55] H. Tedla, I. Díaz, T. Kebede, A.M. Taddesse, Synthesis, characterization and photocatalytic activity of zeolite supported ZnO/Fe2O3/MnO2 nanocomposites, Journal of Environmental Chemical Engineering 3(3) (2015) 1586-1591.
[56] S.A. Gaware, K.A. Rokade, S.N. Kale, Silica-chitosan nanocomposite mediated pH-sensitive drug delivery, Journal of Drug Delivery Science and Technology 49 (2019) 345-351.
[57] A. Enotiadis, N.J. Fernandes, N.A. Becerra, M. Zammarano, E.P. Giannelis, Nanocomposite electrolytes for lithium batteries with reduced flammability, Electrochimica Acta 269 (2018) 76-82.
[58] M. Moghayedi, E.K. Goharshadi, K. Ghazvini, H. Ahmadzadeh, L. Ranjbaran, R. Masoudi, R. Ludwig, Kinetics and mechanism of antibacterial activity and cytotoxicity of Ag-RGO nanocomposite, Colloids and Surfaces B: Biointerfaces 159 (2017) 366-374.
[59] S. Ferraris, S. Spriano, Antibacterial titanium surfaces for medical implants, Materials Science and Engineering: C 61 (2016) 965-978.

[60] B. Aydin Sevinç, L. Hanley, Antibacterial activity of dental composites containing zinc oxide nanoparticles, Journal of Biomedical Materials Research Part B: Applied Biomaterials 94B(1) (2010) 22-31.
[61] J.R. Morones, J.L. Elechiguerra, A. Camacho, K. Holt, J.B. Kouri, J.T. Ramírez, M.J. Yacaman, The bactericidal effect of silver nanoparticles, Nanotechnology 16(10) (2005) 2346.
[62] A.B. Smetana, K.J. Klabunde, G.R. Marchin, C.M. Sorensen, Biocidal activity of nanocrystalline silver powders and particles, Langmuir 24(14) (2008) 7457-7464.
[63] O. Akhavan, E. Ghaderi, Cu and CuO nanoparticles immobilized by silica thin films as antibacterial materials and photocatalysts, Surface and Coatings Technology 205(1) (2010) 219-223.
[64] O. Akhavan, Lasting antibacterial activities of Ag–TiO2/Ag/a-TiO2 nanocomposite thin film photocatalysts under solar light irradiation, Journal of Colloid and Interface Science 336(1) (2009) 117-124.
[65] G. Gosheger, J. Hardes, H. Ahrens, A. Streitburger, H. Buerger, M. Erren, A. Gunsel, F.H. Kemper, W. Winkelmann, C. von Eiff, Silver-coated megaendoprostheses in a rabbit model—an analysis of the infection rate and toxicological side effects, Biomaterials 25(24) (2004) 5547-5556.
[66] P.-o. Rujitanaroj, N. Pimpha, P. Supaphol, Wound-dressing materials with antibacterial activity from electrospun gelatin fiber mats containing silver nanoparticles, Polymer 49(21) (2008) 4723-4732.
[67] D.V. Parikh, T. Fink, K. Rajasekharan, N.D. Sachinvala, A.P.S. Sawhney, T.A. Calamari, A.D. Parikh, Antimicrobial Silver/Sodium Carboxymethyl Cotton Dressings for Burn Wounds, Textile Research Journal 75(2) (2005) 134-138.
[68] J. Ma, J. Zhang, Z. Xiong, Y. Yong, X.S. Zhao, Preparation, characterization and antibacterial properties of silver-modified graphene oxide, Journal of Materials Chemistry 21(10) (2011) 3350-3352.
[69] Q. Yue, Y. Zhang, C. Wang, X. Wang, Z. Sun, X.-F. Hou, D. Zhao, Y. Deng, Magnetic yolk–shell mesoporous silica microspheres with supported Au nanoparticles as recyclable high-performance nanocatalysts, Journal of Materials Chemistry A 3(8) (2015) 4586-4594.
[70] P. Saint-Cricq, J. Wang, A. Sugawara-Narutaki, A. Shimojima, T. Okubo, A new synthesis of well-dispersed, core–shell Ag@ SiO 2 mesoporous nanoparticles using amino acids and sugars, Journal of Materials Chemistry B 1(19) (2013) 2451-2454.
[71] V. Ambrogi, A. Donnadio, D. Pietrella, L. Latterini, F.A. Proietti, F. Marmottini, G. Padeletti, S. Kaciulis, S. Giovagnoli, M. Ricci, Chitosan films containing mesoporous SBA-15 supported silver nanoparticles for wound dressing, Journal of Materials Chemistry B 2(36) (2014) 6054-6063.
[72] L. Zhang, M. Han, O.K. Tan, M.S. Tse, Y.X. Wang, C.C. Sze, Facile fabrication of

Ag/C-TiO2 nanoparticles with enhanced visible light photocatalytic activity for disinfection of Escherichia coli and Enterococcus faecalis, Journal of Materials Chemistry B 1(4) (2013) 564-570.
[73] H. Koga, T. Kitaoka, H. Wariishi, In situ synthesis of silver nanoparticles on zinc oxide whiskers incorporated in a paper matrix for antibacterial applications, Journal of Materials Chemistry 19(15) (2009).
[74] S. Stankovich, D.A. Dikin, G.H. Dommett, K.M. Kohlhaas, E.J. Zimney, E.A. Stach, R.D. Piner, S.T. Nguyen, R.S. Ruoff, Graphene-based composite materials, nature 442(7100) (2006) 282.
[75] S. Dutta, C. Ray, S. Sarkar, M. Pradhan, Y. Negishi, T. Pal, Silver nanoparticle decorated reduced graphene oxide (rGO) nanosheet: a platform for SERS based low-level detection of uranyl ion, ACS Appl Mater Interfaces 5(17) (2013) 8724-32.
[76] S. Stankovich, D.A. Dikin, R.D. Piner, K.A. Kohlhaas, A. Kleinhammes, Y. Jia, Y. Wu, S.T. Nguyen, R.S. Ruoff, Synthesis of graphene-based nanosheets via chemical reduction of exfoliated graphite oxide, Carbon 45(7) (2007) 1558-1565.
[77] A. Fujishima, K.J.n. Honda, Electrochemical photolysis of water at a semiconductor electrode, 238(5358) (1972) 37-38.
[78] H.D. MÜLler, F. Steinbach, Decomposition of Isopropyl Alcohol photosensitized by Zinc Oxide, Nature 225(5234) (1970) 728-729.
[79] F.J.N. Steinbach, Influence of metal support and ultraviolet irradiation on the catalytic activity of nickel oxide, 221(5181) (1969) 657-658.
[80] R. Wang, K. Hashimoto, A. Fujishima, M. Chikuni, E. Kojima, A. Kitamura, M. Shimohigoshi, T.J.N. Watanabe, Light-induced amphiphilic surfaces, 388(6641) (1997) 431-432.
[81] M.R. Hoffmann, S.T. Martin, W. Choi, D.W.J.C.r. Bahnemann, Environmental applications of semiconductor photocatalysis, 95(1) (1995) 69-96.
[82] A. Fujishima, X. Zhang, D.A.J.S.s.r. Tryk, TiO2 photocatalysis and related surface phenomena, 63(12) (2008) 515-582.
[83] A. Fujishima, T.N. Rao, D.A.J.J.o.p. Tryk, p.C.P. reviews, Titanium dioxide photocatalysis, 1(1) (2000) 1-21.
[84] S. Sakthivel, B. Neppolian, M. Shankar, B. Arabindoo, M. Palanichamy, V.J.S.e.m. Murugesan, s. cells, Solar photocatalytic degradation of azo dye: comparison of photocatalytic efficiency of ZnO and TiO2, 77(1) (2003) 65-82.
[85] Y. Bu, Z. Chen, W. Li, Using electrochemical methods to study the promotion mechanism of the photoelectric conversion performance of Ag-modified mesoporous g-C3N4 heterojunction material, Applied Catalysis B: Environmental 144 (2014) 622-630.
[86] Y. Yang, W. Guo, Y. Guo, Y. Zhao, X. Yuan, Y. Guo, Fabrication of Z-scheme plasmonic photocatalyst Ag@AgBr/g-C3N4 with enhanced visible-light photocatalytic activity, Journal of Hazardous Materials 271 (2014) 150-159.

[87] X. Shi, Y. Cheng, N.M. Pugno, H. Gao, Tunable water channels with carbon nanoscrolls, Small 6(6) (2010) 739-744.
[88] X. Shi, N.M. Pugno, Y. Cheng, H. Gao, Gigahertz breathing oscillators based on carbon nanoscrolls, Applied Physics Letters 95(16) (2009) 163113.
[89] P. Yadav, S. Warule, J. Jog, S. Ogale, Carbon nanoscrolls by pyrolysis of a polymer, Solid state communications 152(23) (2012) 2092-2095.
[90] X. Chen, L. Li, X. Sun, H.G. Kia, H. Peng, A novel synthesis of graphene nanoscrolls with tunable dimension at a large scale, Nanotechnology 23(5) (2012) 055603.
[91] Z. Xu, M.J. Buehler, Geometry controls conformation of graphene sheets: membranes, ribbons, and scrolls, ACS nano 4(7) (2010) 3869-3876.
[92] J. Zhao, B. Yang, Z. Yang, P. Zhang, Z. Zheng, W. Ren, X. Yan, Facile preparation of large-scale graphene nanoscrolls from graphene oxide sheets by cold quenching in liquid nitrogen, Carbon 79 (2014) 470-477.
[93] Y. Guo, G. Zhao, N. Wu, Y. Zhang, M. Xiang, B. Wang, H. Liu, H. Wu, Efficient Synthesis of Graphene Nanoscrolls for Fabricating Sulfur-Loaded Cathode and Flexible Hybrid Interlayer toward High-Performance Li-S Batteries, ACS Appl Mater Interfaces 8(50) (2016) 34185-34193.
[94] S.F. Braga, V.R. Coluci, S.B. Legoas, R. Giro, D.S. Galvão, R.H. Baughman, Structure and dynamics of carbon nanoscrolls, Nano letters 4(5) (2004) 881-884.
[95] V. Coluci, S. Braga, R. Baughman, D. Galvao, Prediction of the hydrogen storage capacity of carbon nanoscrolls, Physical Review B 75(12) (2007) 125404.
[96] G. Mpourmpakis, E. Tylianakis, G.E. Froudakis, Carbon nanoscrolls: a promising material for hydrogen storage, Nano letters 7(7) (2007) 1893-1897.
[97] J. Wu, H. Li, X. Qi, Q. He, B. Xu, H. Zhang, Graphene Oxide Architectures Prepared by Molecular Combing on Hydrophilic-Hydrophobic Micropatterns, Small 10(11) (2014) 2239-2244.
[98] F. Zeng, Y. Kuang, Y. Wang, Z. Huang, C. Fu, H. Zhou, Facile Preparation of High-Quality Graphene Scrolls from Graphite Oxide by a Microexplosion Method, Advanced Materials 23(42) (2011) 4929-4932.
[99] H. Pan, Y. Feng, J. Lin, Ab initio study of electronic and optical properties of multiwall carbon nanotube structures made up of a single rolled-up graphite sheet, Physical Review B 72(8) (2005) 085415.
[100] Y. Chen, J. Lu, Z. Gao, Structural and electronic study of nanoscrolls rolled up by a single graphene sheet, The Journal of Physical Chemistry C 111(4) (2007) 1625-1630.
[101] Z. Xu, B. Zheng, J. Chen, C. Gao, Highly Efficient Synthesis of Neat Graphene Nanoscrolls from Graphene Oxide by Well-Controlled Lyophilization, Chemistry of Materials 26(23) (2014) 6811-6818.
[102] X. Xie, L. Ju, X. Feng, Y. Sun, R. Zhou, K. Liu, S. Fan, Q. Li, K. Jiang, Controlled fabrication of high-quality carbon nanoscrolls from monolayer graphene, Nano letters 9(7)

(2009) 2565-2570.
[103] J. Zheng, H. Liu, B. Wu, Y. Guo, T. Wu, G. Yu, Y. Liu, D. Zhu, Production of high-quality carbon nanoscrolls with microwave spark assistance in liquid nitrogen, Advanced Materials 23(21) (2011) 2460-2463.
[104] S. Braga, V. Coluci, R. Baughman, D. Galvao, Hydrogen storage in carbon nanoscrolls: An atomistic molecular dynamics study, Chemical physics letters 441(1-3) (2007) 78-82.
[105] L.M. Viculis, J.J. Mack, R.B. Kaner, A chemical route to carbon nanoscrolls, Science 299(5611) (2003) 1361-1361.
[106] H. Shioyama, T. Akita, A new route to carbon nanotubes, Carbon (New York, NY) 41(1) (2003) 179-181.
[107] M.V. Savoskin, V.N. Mochalin, A.P. Yaroshenko, N.I. Lazareva, T.E. Konstantinova, I.V. Barsukov, I.G. Prokofiev, Carbon nanoscrolls produced from acceptor-type graphite intercalation compounds, Carbon 45(14) (2007) 2797-2800.
[108] R. Bacon, Growth, structure, and properties of graphite whiskers, Journal of Applied Physics 31(2) (1960) 283-290.
[109] J. Li, Q. Peng, G. Bai, W. Jiang, Carbon scrolls produced by high energy ball milling of graphite, Carbon (New York, NY) 43(13) (2005) 2830-2833.
[110] M. Yan, F. Wang, C. Han, X. Ma, X. Xu, Q. An, L. Xu, C. Niu, Y. Zhao, X. Tian, Nanowire templated semihollow bicontinuous graphene scrolls: designed construction, mechanism, and enhanced energy storage performance, Journal of the American Chemical Society 135(48) (2013) 18176-18182.
[111] U. Mirsaidov, V. Mokkapati, D. Bhattacharya, H. Andersen, M. Bosman, B. Özyilmaz, P. Matsudaira, Scrolling graphene into nanofluidic channels, Lab on a Chip 13(15) (2013) 2874-2878.
[112] C. Xu, X. Wang, L. Yang, Y. Wu, Fabrication of a graphene–cuprous oxide composite, Journal of Solid State Chemistry 182(9) (2009) 2486-2490.
[113] Y. Cong, T. Xia, M. Zou, Z. Li, B. Peng, D. Guo, Z. Deng, Mussel-inspired polydopamine coating as a versatile platform for synthesizing polystyrene/Ag nanocomposite particles with enhanced antibacterial activities, Journal of Materials Chemistry B 2(22) (2014) 3450-3461.
[114] Z. Zhang, J. Zhang, B. Zhang, J. Tang, Mussel-inspired functionalization of graphene for synthesizing Ag-polydopamine-graphene nanosheets as antibacterial materials, Nanoscale 5(1) (2013) 118-123.
[115] W. Hu, C. Peng, W. Luo, M. Lv, X. Li, D. Li, Q. Huang, C. Fan, Graphene-based antibacterial paper, ACS nano 4(7) (2010) 4317-4323.
[116] C. Carlson, S.M. Hussain, A.M. Schrand, L. K. Braydich-Stolle, K.L. Hess, R.L. Jones, J.J. Schlager, Unique cellular interaction of silver nanoparticles: size-dependent generation of reactive oxygen species, The journal of physical chemistry B 112(43) (2008)

13608-13619.
[117] F. Martínez-Gutierrez, E.P. Thi, J.M. Silverman, C.C. de Oliveira, S.L. Svensson, A.V. Hoek, E.M. Sánchez, N.E. Reiner, E.C. Gaynor, E.L. Pryzdial, Antibacterial activity, inflammatory response, coagulation and cytotoxicity effects of silver nanoparticles, Nanomedicine: Nanotechnology, Biology and Medicine 8(3) (2012) 328-336.
[118] J. Chen, Y. Li, L. Huang, C. Li, G. Shi, High-yield preparation of graphene oxide from small graphite flakes via an improved Hummers method with a simple purification process, Carbon 81 (2015) 826-834.
[119] X. Yan, S. Li, J. Bao, N. Zhang, B. Fan, R. Li, X. Liu, Y.-X. Pan, Immobilization of Highly Dispersed Ag Nanoparticles on Carbon Nanotubes Using Electron-Assisted Reduction for Antibacterial Performance, ACS Applied Materials & Interfaces 8(27) (2016) 17060-17067.
[120] W. Xu, W. Jin, L. Lin, C. Zhang, Z. Li, Y. Li, R. Song, B. Li, Green synthesis of xanthan conformation-based silver nanoparticles: Antibacterial and catalytic application, Carbohydrate Polymers 101 (2014) 961-967.
[121] S.J. Kazmi, M.A. Shehzad, S. Mehmood, M. Yasar, A. Naeem, A.S. Bhatti, Effect of varied Ag nanoparticles functionalized CNTs on its anti-bacterial activity against E. coli, Sensors and Actuators A: Physical 216 (2014) 287-294.
[122] Y.W. Wang, A. Cao, Y. Jiang, X. Zhang, J.H. Liu, Y. Liu, H. Wang, Superior antibacterial activity of zinc oxide/graphene oxide composites originating from high zinc concentration localized around bacteria, ACS Appl Mater Interfaces 6(4) (2014) 2791-8.
[123] H. Wang, Q. Wei, X. Wang, W. Gao, X. Zhao, Antibacterial properties of PLA nonwoven medical dressings coated with nanostructured silver, Fibers and Polymers 9(5) (2008) 556-560.
[124] Q. Guan, C. Xia, W. Li, Bio-friendly controllable synthesis of silver nanoparticles and their enhanced antibacterial property, Catalysis Today 327 (2019) 196-202.
[125] J. Bae, H. Kwon, J. Kim, Safety evaluation of absorbent hygiene pads: a review on assessment framework and test methods, Sustainability 10(11) (2018) 4146.
[126] P. Huang, J. Lin, Z. Li, H. Hu, K. Wang, G. Gao, R. He, D. Cui, A general strategy for metallic nanocrystals synthesis in organic medium, Chemical Communications 46(26) (2010) 4800-4802.
[127] A. Bagri, C. Mattevi, M. Acik, Y.J. Chabal, M. Chhowalla, V.B. Shenoy, Structural evolution during the reduction of chemically derived graphene oxide, Nature chemistry 2(7) (2010) 581-587.
[128] L. Shahriary, A.A. Athawale, Graphene oxide synthesized by using modified hummers approach, Int. J. Renew. Energy Environ. Eng 2(01) (2014) 58-63.
[129] K. De Silva, H.-H. Huang, R. Joshi, M. Yoshimura, Chemical reduction of graphene oxide using green reductants, Carbon 119 (2017) 190-199.
[130] L. Fu, H.-b. LIU, Y.-h. ZOU, B. LI, TECHNOLOGY RESEARCH ON

OXIDATIVE DEGREE OF GRAPHITE OXIDE PREPARED BY HUMMERS METHOD [J], Carbon 4 (2005) 10-14.
[131] K.-S. Chou, Y.-S. Lai, Effect of polyvinyl pyrrolidone molecular weights on the formation of nanosized silver colloids, Materials Chemistry and Physics 83(1) (2004) 82-88.
[132] A.S. Goldman, Carbon–carbon bonds get a break, Nature 463(7280) (2010) 435.
[133] A. Sattler, G. Zhu, G. Parkin, Multiple Modes for Coordination of Phenazine to Molybdenum: Ring Fusion Promotes Access to η4-Coordination, Oxidative Addition of Dihydrogen and Hydrogenation of Aromatic Nitrogen Compounds, Journal of the American Chemical Society 131(22) (2009) 7828-7838.
[134] K.S. Rutkowski, W.A. Herrebout, S.M. Melikova, B.J. van der Veken, A. Koll, A cryosolution FTIR and ab initio study of the blue shifting C–H···F hydrogen bonded complexes F2ClCH·FCD3 and Cl2FCH·FCD3, Chemical Physics 354(1) (2008) 71-79.
[135] J. Natsuki, T. Abe, Synthesis of pure colloidal silver nanoparticles with high electroconductivity for printed electronic circuits: The effect of amines on their formation in aqueous media, Journal of Colloid and Interface Science 359(1) (2011) 19-23.
[136] L. Ye, J. Liu, C. Gong, L. Tian, T. Peng, L. Zan, Two different roles of metallic Ag on Ag/AgX/BiOX (X= Cl, Br) visible light photocatalysts: surface plasmon resonance and Z-scheme bridge, Acs Catalysis 2(8) (2012) 1677-1683.
[137] C. Chen, W. Ma, J. Zhao, Semiconductor-mediated photodegradation of pollutants under visible-light irradiation, Chemical Society Reviews 39(11) (2010) 4206-4219.
[138] A.L. Linsebigler, G. Lu, J.T. Yates Jr, Photocatalysis on TiO2 surfaces: principles, mechanisms, and selected results, Chemical reviews 95(3) (1995) 735-758.
[139] W. Teng, X. Li, Q. Zhao, J. Zhao, D. Zhang, In situ capture of active species and oxidation mechanism of RhB and MB dyes over sunlight-driven Ag/Ag3PO4 plasmonic nanocatalyst, Applied Catalysis B: Environmental 125 (2012) 538-545.
[140] H. Park, W. Choi, Visible light and Fe (III)-mediated degradation of Acid Orange 7 in the absence of H2O2, Journal of Photochemistry and Photobiology A: Chemistry 159(3) (2003) 241-247.
[141] I.K. Konstantinou, T.A. Albanis, TiO2-assisted photocatalytic degradation of azo dyes in aqueous solution: kinetic and mechanistic investigations: a review, Applied Catalysis B: Environmental 49(1) (2004) 1-14.
[142] A. Kar, Y.R. Smith, V. Subramanian, Improved photocatalytic degradation of textile dye using titanium dioxide nanotubes formed over titanium wires, Environmental science & technology 43(9) (2009) 3260-3265.
[143] F.J. Cervantes, A. Garcia-Espinosa, M.A. Moreno-Reynosa, J.R. Rangel-Mendez, Immobilized redox mediators on anion exchange resins and their role on the reductive decolorization of azo dyes, Environmental science & technology 44(5) (2010) 1747-1753.
[144] C.E. Clarke, F. Kielar, H.M. Talbot, K.L. Johnson, Oxidative decolorization of acid

azo dyes by a Mn oxide containing waste, Environmental science & technology 44(3) (2010) 1116-1122.
[145] Y. Liu, G. Zhu, J. Gao, R. Zhu, M. Hojamberdiev, C. Wang, X. Wei, P. Liu, A novel synergy of Er3+/Fe3+ co-doped porous Bi5O7I microspheres with enhanced photocatalytic activity under visible-light irradiation, Applied Catalysis B: Environmental 205 (2017) 421-432.
[146] Q. Wang, J. He, Y. Shi, S. Zhang, T. Niu, H. She, Y. Bi, Z. Lei, Synthesis of MFe2O4 (M= Ni, Co)/BiVO4 film for photolectrochemical hydrogen production activity, Applied Catalysis B: Environmental 214 (2017) 158-167.
[147] Y. Chen, G. Zhu, M. Hojamberdiev, J. Gao, R. Zhu, C. Wang, X. Wei, P. Liu, Three-dimensional Ag2O/Bi5O7I p–n heterojunction photocatalyst harnessing UV–vis–NIR broad spectrum for photodegradation of organic pollutants, Journal of hazardous materials 344 (2018) 42-54.
[148] I.H. Alsohaimi, A.M. Nassar, T.A. Seaf Elnasr, B.a. Cheba, A novel composite silver nanoparticles loaded calcium oxide stemming from egg shell recycling: A potent photocatalytic and antibacterial activities, Journal of Cleaner Production 248 (2020).
[149] N.T. Khoa, S.W. Kim, D.-H. Yoo, S. Cho, E.J. Kim, S.H. Hahn, Fabrication of Au/graphene-wrapped ZnO-nanoparticle-assembled hollow spheres with effective photoinduced charge transfer for photocatalysis, ACS applied materials & interfaces 7(6) (2015) 3524-3531.
[150] K. Bramhaiah, V.N. Singh, N.S. John, Hybrid materials of ZnO nanostructures with reduced graphene oxide and gold nanoparticles: enhanced photodegradation rates in relation to their composition and morphology, Physical Chemistry Chemical Physics 18(3) (2016) 1478-1486.
[151] C. Santhosh, V. Velmurugan, G. Jacob, S.K. Jeong, A.N. Grace, A. Bhatnagar, Role of nanomaterials in water treatment applications: a review, Chemical Engineering Journal 306 (2016) 1116-1137.
[152] Y. Chi, J. Tu, M. Wang, X. Li, Z. Zhao, One-pot synthesis of ordered mesoporous silver nanoparticle/carbon composites for catalytic reduction of 4-nitrophenol, Journal of colloid and interface science 423 (2014) 54-59.
[153] M. Wang, J. Fu, D. Huang, C. Zhang, Q. Xu, Silver nanoparticles-decorated polyphosphazene nanotubes: synthesis and applications, Nanoscale 5(17) (2013) 7913-7919.
[154] M. Rycenga, C.M. Cobley, J. Zeng, W. Li, C.H. Moran, Q. Zhang, D. Qin, Y. Xia, Controlling the synthesis and assembly of silver nanostructures for plasmonic applications, Chemical reviews 111(6) (2011) 3669-3712.
[155] J. Zheng, H. Lin, X. Zheng, X. Duan, Y. Yuan, Highly efficient mesostructured Ag/SBA-15 catalysts for the chemoselective synthesis of methyl glycolate by dimethyl oxalate hydrogenation, Catalysis Communications 40 (2013) 129-133.

[156] X. Chen, J. Lei, Y. Wang, W. Zhu, W. Yao, T. Duan, Ternary Ag nanoparticles/natural-magnetic SiO 2-nanowires/reduced graphene oxide nanocomposites with highly visible photocatalytic activity for 4-nitrophenol reduction, SN Applied Sciences 1(1) (2019) 130.
[157] C. Wang, Z. Zhang, G. Yang, Q. Chen, Y. Yin, M. Jin, Creation of controllable high-density defects in silver nanowires for enhanced catalytic property, Nano letters 16(9) (2016) 5669-5674.
[158] P. Zhang, C. Shao, Z. Zhang, M. Zhang, J. Mu, Z. Guo, Y. Liu, In situ assembly of well-dispersed Ag nanoparticles (AgNPs) on electrospun carbon nanofibers (CNFs) for catalytic reduction of 4-nitrophenol, Nanoscale 3(8) (2011) 3357-3363.
[159] B. Naik, S. Hazra, V.S. Prasad, N.N. Ghosh, Synthesis of Ag nanoparticles within the pores of SBA-15: an efficient catalyst for reduction of 4-nitrophenol, Catalysis Communications 12(12) (2011) 1104-1108.
[160] N.T. Khoa, S.W. Kim, D. Van Thuan, H.N. Tien, S.H. Hur, E.J. Kim, S.H. Hahn, Fast and effective electron transport in a Au–graphene–ZnO hybrid for enhanced photocurrent and photocatalysis, RSC Advances 5(78) (2015) 63964-63969.
[161] P. Wang, D. Wu, Y. Ao, C. Wang, J. Hou, ZnO nanorod arrays co-loaded with Au nanoparticles and reduced graphene oxide: Synthesis, characterization and photocatalytic application, Colloids and Surfaces A: Physicochemical and Engineering Aspects 492 (2016) 71-78.
[162] R. Madhu, B. Dinesh, S.-M. Chen, R. Saraswathi, V. Mani, An electrochemical synthesis strategy for composite based ZnO microspheres–Au nanoparticles on reduced graphene oxide for the sensitive detection of hydrazine in water samples, RSC Advances 5(67) (2015) 54379-54386.
[163] Y. Zhang, C. Zhao, Z. Zeng, J.M. Ang, B. Che, Z. Wang, X. Lu, Graphene nanoscroll/nanosheet aerogels with confined SnS2 nanosheets: simultaneous wrapping and bridging for high-performance lithium-ion battery anodes, Electrochimica Acta 278 (2018) 156-164.
[164] B.M. Pirzada, Pushpendra, R.K. Kunchala, B.S. Naidu, Synthesis of LaFeO3/Ag2CO3 Nanocomposites for Photocatalytic Degradation of Rhodamine B and p-Chlorophenol under Natural Sunlight, ACS Omega 4(2) (2019) 2618-2629.
[165] B. Zhou, X. Zhao, H. Liu, J. Qu, C.P. Huang, Visible-light sensitive cobalt-doped BiVO4 (Co-BiVO4) photocatalytic composites for the degradation of methylene blue dye in dilute aqueous solutions, Applied Catalysis B: Environmental 99(1-2) (2010) 214-221.
[166] B.M. Pirzada, O. Mehraj, N.A. Mir, M.Z. Khan, S. Sabir, Efficient visible light photocatalytic activity and enhanced stability of BiOBr/Cd (OH) 2 heterostructures, New Journal of Chemistry 39(9) (2015) 7153-7163.
[167] A. Kudo, Y. Miseki, Heterogeneous photocatalyst materials for water splitting, Chemical Society Reviews 38(1) (2009) 253-278.

[168] D. Rajamanickam, M. Shanthi, Photocatalytic degradation of an organic pollutant by zinc oxide – solar process, Arabian Journal of Chemistry 9 (2016) S1858-S1868.
[169] M.A. Rauf, S.S. Ashraf, Fundamental principles and application of heterogeneous photocatalytic degradation of dyes in solution, Chemical Engineering Journal 151(1) (2009) 10-18.
[170] Y. Ma, J.-N.J.C. Yao, Comparison of photodegradative rate of rhodamine B assisted by two kinds of TI02 films, 38(10) (1999) 2407-2414.
[171] L. Andronic, L. Isac, S. Miralles-Cuevas, M. Visa, I. Oller, A. Duta, S.J.J.o.H.m. Malato, Pilot-plant evaluation of TiO2 and TiO2-based hybrid photocatalysts for solar treatment of polluted water, 320 (2016) 469-478.
[172] J.-M. Wu, T.-W.J.J.o.P. Zhang, P.A. Chemistry, Photodegradation of rhodamine B in water assisted by titania films prepared through a novel procedure, 162(1) (2004) 171-177.
[173] S. Rasalingam, C.-M. Wu, R.T. Koodali, Modulation of Pore Sizes of Titanium Dioxide Photocatalysts by a Facile Template Free Hydrothermal Synthesis Method: Implications for Photocatalytic Degradation of Rhodamine B, ACS Applied Materials & Interfaces 7(7) (2015) 4368-4380.
[174] J.-A. Park, B. Yang, J. Lee, I.G. Kim, J.-H. Kim, J.-W. Choi, H.-D. Park, I.W. Nah, S.-H. Lee, Ultrasonic spray pyrolysis synthesis of reduced graphene oxide/anatase TiO2 composite and its application in the photocatalytic degradation of methylene blue in water, Chemosphere 191 (2018) 738-746.
[175] Y. Haldorai, J.J. Shim, Novel chitosan-TiO2 nanohybrid: Preparation, characterization, antibacterial, and photocatalytic properties, Polymer Composites 35(2) (2014) 327-333.
[176] A. Phuruangrat, S. Thongtem, T. Thongtem, Ultrasonic-assisted synthesis and photocatalytic performance of ZnO nanoplates and microflowers, Materials & Design 107 (2016) 250-256.
[177] Q. Qi, S. Liu, X. Li, C. Kong, Z. Guo, L. Chen, In situ fabrication of ZnO@N-doped nanoporous carbon core-shell heterostructures with high photocatalytic and adsorption capacity by a calcination of ZnO@MOF strategy, Journal of Solid State Chemistry 255 (2017) 108-114.
[178] N. Atar, T. Eren, M.L. Yola, H. Karimi-Maleh, B. Demirdögen, Magnetic iron oxide and iron oxide@ gold nanoparticle anchored nitrogen and sulfur-functionalized reduced graphene oxide electrocatalyst for methanol oxidation, RSC Advances 5(33) (2015) 26402-26409.
[179] M.L. Yola, N. Atar, T. Eren, H. Karimi-Maleh, S. Wang, Correction: Sensitive and selective determination of aqueous triclosan based on gold nanoparticles on polyoxometalate/reduced graphene oxide nanohybrid, RSC Advances 5(89) (2015) 72590-72591.

[180] F. Lorestani, P.M. Nia, Y. Alias, N.S. Manan, One-step synthesis of different silver-polyaniline composite morphologies for enzymless hydrogen peroxide detection, Journal of The Electrochemical Society 162(7) (2015) B193-B200.
[181] M.L. Yola, N. Atar, Z. Üstündağ, A.O. Solak, A novel voltammetric sensor based on p-aminothiophenol functionalized graphene oxide/gold nanoparticles for determining quercetin in the presence of ascorbic acid, Journal of Electroanalytical Chemistry 698 (2013) 9-16.
[182] G. Ghodake, D.-Y. Kim, J.H. Jo, J. Jang, D.S. Lee, One-step green synthesis of gold nanoparticles using casein hydrolytic peptides and their anti-cancer assessment using the DU145 cell line, Journal of Industrial and Engineering Chemistry 33 (2016) 185-189.
[183] A. Ahmad, F. Syed, A. Shah, Z. Khan, K. Tahir, A.U. Khan, Q. Yuan, Silver and gold nanoparticles from Sargentodoxa cuneata: synthesis, characterization and antileishmanial activity, RSC Advances 5(90) (2015) 73793-73806.
[184] Y. Li, F. Qian, J. Xiang, C.M. Lieber, Nanowire electronic and optoelectronic devices, Materials today 9(10) (2006) 18-27.
[185] O.K. Varghese, C.A. Grimes, Metal oxide nanoarchitectures for environmental sensing, Journal of nanoscience and nanotechnology 3(4) (2003) 277-293.
[186] G. Shen, P.-C. Chen, K. Ryu, C. Zhou, Devices and chemical sensing applications of metal oxide nanowires, Journal of Materials Chemistry 19(7) (2009) 828-839.
[187] M. Chandra, Q. Xu, Room temperature hydrogen generation from aqueous ammonia-borane using noble metal nano-clusters as highly active catalysts, Journal of Power Sources 168(1) (2007) 135-142.
[188] S. Maier, M. Brongersma, P. Kik, S. Meltzer, A. Requicha, B. Koel, H. Atwater, Plasmonics—A route to nanoscale optical devices (Advanced Materials, 2001, 13, 1501), Advanced materials 15(7-8) (2003) 562-562.
[189] R. Qiu, H.G. Cha, H.B. Noh, Y.B. Shim, X.L. Zhang, R. Qiao, D. Zhang, Y.I. Kim, U. Pal, Y.S. Kang, Preparation of dendritic copper nanostructures and their characterization for electroreduction, The Journal of Physical Chemistry C 113(36) (2009) 15891-15896.
[190] S. Xu, B. Man, S. Jiang, J. Wang, J. Wei, S. Xu, H. Liu, S. Gao, H. Liu, Z. Li, H. Li, H. Qiu, Graphene/Cu Nanoparticle Hybrids Fabricated by Chemical Vapor Deposition As Surface-Enhanced Raman Scattering Substrate for Label-Free Detection of Adenosine, ACS Applied Materials & Interfaces 7(20) (2015) 10977-10987.
[191] F. Meng, W. Shi, Y. Sun, X. Zhu, G. Wu, C. Ruan, X. Liu, D. Ge, Nonenzymatic biosensor based on CuxO nanoparticles deposited on polypyrrole nanowires for improving detectionrange, Biosensors and Bioelectronics 42 (2013) 141-147.
[192] P. Moozarm Nia, P.M. Woi, Y. Alias, Facile one-step electrochemical deposition of copper nanoparticles and reduced graphene oxide as nonenzymatic hydrogen peroxide sensor, Applied Surface Science 413 (2017) 56-65.

[193] N.A. Luechinger, E.K. Athanassiou, W.J. Stark, Graphene-stabilized copper nanoparticles as an air-stable substitute for silver and gold in low-cost ink-jet printable electronics, Nanotechnology 19(44) (2008) 445201.
[194] A.D. Brumbaugh, K.A. Cohen, S.K. St. Angelo, Ultrasmall copper nanoparticles synthesized with a plant tea reducing agent, ACS Sustainable Chemistry & Engineering 2(8) (2014) 1933-1939.
[195] M.M. Hasan, S.A. Tolba, N.K. Allam, In Situ Formation of Graphene Stabilizes Zero-Valent Copper Nanoparticles and Significantly Enhances the Efficiency of Photocatalytic Water Splitting, ACS Sustainable Chemistry & Engineering 6(12) (2018) 16876-16885.
[196] A.T. Simon, D. Dutta, A. Chattopadhyay, S.S. Ghosh, Copper Nanocluster-Doped Luminescent Hydroxyapatite Nanoparticles for Antibacterial and Antibiofilm Applications, ACS Omega 4(3) (2019) 4697-4706.
[197] X. Liu, Y. Zhou, Electrochemical synthesis and room temperature oxidation behavior of Cu nanowires, Journal of materials research 20(9) (2005) 2371-2378.
[198] C.-H. Chen, T. Yamaguchi, K.-i. Sugawara, K. Koga, Role of stress in the self-limiting oxidation of copper nanoparticles, The Journal of Physical Chemistry B 109(44) (2005) 20669-20672.
[199] P. Pulkkinen, J. Shan, K. Leppanen, A. Kansakoski, A. Laiho, M. Jarn, H. Tenhu, Poly (ethylene imine) and tetraethylenepentamine as protecting agents for metallic copper nanoparticles, ACS applied materials & interfaces 1(2) (2009) 519-525.
[200] C. Mattevi, H. Kim, M. Chhowalla, A review of chemical vapour deposition of graphene on copper, Journal of Materials Chemistry 21(10) (2011) 3324-3334.
[201] M. Grouchko, A. Kamyshny, S. Magdassi, Formation of air-stable copper–silver core–shell nanoparticles for inkjet printing, Journal of Materials Chemistry 19(19) (2009) 3057-3062.
[202] M. Grouchko, A. Kamyshny, K. Ben-Ami, S. Magdassi, Synthesis of copper nanoparticles catalyzed by pre-formed silver nanoparticles, Journal of Nanoparticle Research 11(3) (2009) 713-716.
[203] Z. Dong, X. Le, X. Li, W. Zhang, C. Dong, J. Ma, Silver nanoparticles immobilized on fibrous nano-silica as highly efficient and recyclable heterogeneous catalyst for reduction of 4-nitrophenol and 2-nitroaniline, Applied Catalysis B: Environmental 158-159 (2014) 129-135.
[204] H.K. Hareesh, R.P. Joshi, S. D.V, V.N. Bhoraskar, S.D. Dhole, Anchoring of Ag-Au alloy nanoparticles on reduced graphene oxide sheets for the reduction of 4-nitrophenol, Applied Surface Science 389 (2016) 1050-1055.
[205] D. Prasai, J.C. Tuberquia, R.R. Harl, G.K. Jennings, B.R. Rogers, K.I. Bolotin, Correction to graphene: corrosion-inhibiting coating, ACS nano 6(5) (2012) 4540-4540.
[206] S. Wang, X. Huang, Y. He, H. Huang, Y. Wu, L. Hou, X. Liu, T. Yang, J. Zou, B.

Huang, Synthesis, growth mechanism and thermal stability of copper nanoparticles encapsulated by multi-layer graphene, Carbon 50(6) (2012) 2119-2125.
[207] X. Guo, C. Hao, G. Jin, H.Y. Zhu, X.Y. Guo, Copper nanoparticles on graphene support: an efficient photocatalyst for coupling of nitroaromatics in visible light, Angew Chem Int Ed Engl 53(7) (2014) 1973-7.
[208] L. Jin, G. He, J. Xue, T. Xu, H. Chen, Cu/graphene with high catalytic activity prepared by glucose blowing for reduction of p -nitrophenol, Journal of Cleaner Production 161 (2017) 655-662.
[209] X. Li, W. Cai, J. An, S. Kim, J. Nah, D. Yang, R. Piner, A. Velamakanni, I. Jung, E. Tutuc, Large-area synthesis of high-quality and uniform graphene films on copper foils, science 324(5932) (2009) 1312-1314.
[210] J.-W. Rhim, Effect of PLA lamination on performance characteristics of agar/κ-carrageenan/clay bio-nanocomposite film, Food Research International 51(2) (2013) 714-722.
[211] J.W. Rhim, L.F. Wang, S.I. Hong, Preparation and characterization of agar/silver nanoparticles composite films with antimicrobial activity, Food Hydrocolloids 33(2) (2013) 327-335.
[212] J.P. Reddy, J.-W. Rhim, Characterization of bionanocomposite films prepared with agar and paper-mulberry pulp nanocellulose, Carbohydrate Polymers 110 (2014) 480-488.
[213] Y. Lee, J.-r. Choi, K.J. Lee, N.E. Stott, D. Kim, Large-scale synthesis of copper nanoparticles by chemically controlled reduction for applications of inkjet-printed electronics, Nanotechnology 19(41) (2008) 415604.
[214] N. Leopold, B. Lendl, A New Method for Fast Preparation of Highly Surface-Enhanced Raman Scattering (SERS) Active Silver Colloids at Room Temperature by Reduction of Silver Nitrate with Hydroxylamine Hydrochloride, The Journal of Physical Chemistry B 107(24) (2003) 5723-5727.
[215] Y. Tan, X. Dai, Y. Li, D. Zhu, Preparation of gold, platinum, palladium and silver nanoparticles by the reduction of their salts with a weak reductant–potassium bitartrate, Journal of Materials Chemistry 13(5) (2003) 1069-1075.
[216] J. Xiong, Y. Wang, Q. Xue, X. Wu, Synthesis of highly stable dispersions of nanosized copper particles using l-ascorbic acid, Green Chemistry 13(4) (2011).
[217] S. Wu, Preparation of fine copper powder using ascorbic acid as reducing agent and its application in MLCC, Materials Letters 61(4-5) (2007) 1125-1129.
[218] G. Cheng, A.H. Walker, Transmission electron microscopy characterization of colloidal copper nanoparticles and their chemical reactivity, Analytical and bioanalytical chemistry 396(3) (2010) 1057-1069.
[219] L. Fu, H.-b. LIU, Y.-h. ZOU, B. LI, Technology research on oxidative degree of graphite oxide prepared by Hummers method, Carbon 4 (2005) 10-14.
[220] L. Hang, Y. Zhao, H. Zhang, G. Liu, W. Cai, Y. Li, L. Qu, Copper

nanoparticle@graphene composite arrays and their enhanced catalytic performance, Acta Materialia 105 (2016) 59-67.
[221] L. Tang, L. Zhu, F. Tang, C. Yao, J. Wang, L. Li, Mild Synthesis of Copper Nanoparticles with Enhanced Oxidative Stability and Their Application in Antibacterial Films, Langmuir 34(48) (2018) 14570-14576.
[222] C. Castiglioni, M. Tommasini, G. Zerbi, Raman spectroscopy of polyconjugated molecules and materials: Confinement effect in one and two dimensions, Philosophical Transactions of the Royal Society A: Mathematical, Physical and Engineering Sciences 362(1824) (2004) 2425-2459.
[223] R. Jiang, X. Zhou, Q. Fang, Z. Liu, Copper–graphene bulk composites with homogeneous graphene dispersion and enhanced mechanical properties, Materials Science and Engineering: A 654 (2016) 124-130.
[224] C. Castiglioni, F. Negri, M. Rigolio, G. Zerbi, Raman activation in disordered graphites of the A′1 symmetry forbidden k≠0 phonon: The origin of the D line, Journal of Chemical Physics 115(8) (2001) 3769-3778.
[225] K.M. Liew, X.Q. He, S. Kitipornchai, Predicting nanovibration of multi-layered graphene sheets embedded in an elastic matrix, Acta Materialia 54(16) (2006) 4229-4236.
[226] A.A. Radhakrishnan, B.B. Beena, Structural and optical absorption analysis of CuO nanoparticles, Indian Journal of Advances in Chemical Science 2(2) (2014) 158-161.
[227] S. Jeong, K. Woo, D. Kim, S. Lim, J.S. Kim, H. Shin, Y. Xia, J. Moon, Controlling the thickness of the surface oxide layer on Cu nanoparticles for the fabrication of conductive structures by ink-jet printing, Advanced Functional Materials 18(5) (2008) 679-686.

Acknowledgements

It is my great pleasure to thank the persons who give me help and advice with the thesis. Here, I want to give my most sincere gratitude to them.

First and foremost, I would like to thank my supervisor Prof. Toshiaki Natsuki. He gives me the most important supports and patience for my research and living. His advice helps me to overcome several key problems in my work and teaches me how to write a scientific paper in a strict manner. Thanks to his guidance, I can complete my PhD.

I am also grateful to Dr. Jun Natsuki for her guidance and valuable suggestion in the study.

I am also grateful to Prof. Qing-Qing Ni for his help for my research and living. Thank the Group of Yasuo Goto for his help of TGA experiments.

I want to express my gratitude to Shinshu University for the support, and the members of Sakukosumosu Rotary Club especially my counselor, Norihiko Shiratori, for supplying my scholarship and helping me learn about more Japanese culture.

I want to thank the technicians in our group, Nakamura, and other technicians in our campus, especially Nakamura, for their kindness and help.

I must thank all former and current members of my group mates. Hairong Chen, Xiaoyu Guan, Yongjie Yan, Jun Hong, Jing Hui, Yinan Jing, Yajun Liu, Canyi Huang, Lina Cui, Si Chen, Chongchao Li, and Ping Xu. Thanks to their help for my PhD.

Finally, I would like to thanks my parents. They always support me completely so that I have the opportunity to go all out for what I desired without any hesitation. This thesis would not have been possible without the love of my family.